THE PROPAGATION AND ARREST OF AN EDGE CRACK IN AN ELASTIC HALF-SPACE UNDER CONDITIONS OF ANTI-PLANE SHEAR: ANALYTICAL AND NUMERICAL RESULTS

Thesis by
Timothy Christopher O'Sullivan

In Partial Fulfillment of the Requirements
for the Degree of
Doctor of Philosophy

California Institute of Technology
Pasadena, California
1983

(Submitted October 26, 1982)

ACKNOWLEDGMENTS

I would like to express my sincere appreciation and gratitude to Professor J.K. Knowles for his assistance and encouragement during the course of this investigation. I would also like to thank Professor H. B. Keller for a number of helpful discussions on the numerical work.

The author is very grateful for the Earle C. Anthony Fellowship, the teaching assistantships, and the tuition scholarships granted to him by the California Institute of Technology as well as the financial support received from the Office of Naval Research while this work was in progress.

Special thanks go to Rennie Dudek for her care and patience in typing this thesis and to Cecilia Lin for her work on the figures. Finally to all my friends in Caltech over the past four years, I wish to convey my gratitude for their help and friendship.

Summary

The motion of an edge crack extending non-uniformly in an elastic half-space under conditions of anti-plane shear is analyzed. An expression for the stress intensity factor at the crack tip is obtained, and an energy balance crack propagation criterion is used to find the equation of motion of the tip. On solving this equation numerically, it is found that crack arrest occurs before the second reflected wave from the boundary reaches the tip.

In the second half of this investigation, a numerical procedure for studying anti-plane shear crack propagation problems using finite differences is developed. To approximate the elastodynamic field as accurately as possible near the moving crack tip, where singular stresses occur, the local asymptotic displacement field near the tip is incorporated into the finite difference scheme. The numerical procedure is applied to the edge crack problem analyzed in the first part of this study, and the numerical and exact results are compared.

TABLE OF CONTENTS

GENERAL INTRODUCTION

The analysis of rapid crack propagation and crack arrest in solid bodies has recently been generating a considerable amount of interest. Generally the failure of a structure through fracture is avoided by preventing the onset of unstable crack growth. This can be done by ensuring that the stresses do not exceed certain material-dependent limits imposed by critical flaw sizes in the material. However excluding unstable crack extension under a wide range of operating conditions can often be very difficult and costly. A suitable second measure of safety would be to ensure the timely arrest of a propagating crack and this is often a practical necessity in important structures such as nuclear pressure vessels, welded ships and pressurized pipelines. In cases like these, unstable crack propagation without arrest could have very serious consequences.

Dynamic crack propagation problems generally fall into two categories. Firstly, for prescribed crack history, the elastodynamic field in the body is to be determined. Alternatively, for an unstable crack in a body, given all the necessary information concerning the geometry, the loads and the material of which the body is composed, together with a crack propagation criterion as well, one can attempt to determine the subsequent motion of the crack. The latter case will concern us in this study.

Now the rapid motion of a crack in a body introduces inertia effects in the form of stress waves radiating outward from the moving crack tip. Hence in analyzing a dynamic fracture problem, the reflections and diffractions of these stress waves by the material boundaries and by the

crack itself must be taken into account. Because of the inherent mathematical difficulty in the boundary-initial value problem due to the presence of the propagating crack and the disturbances caused by these wave motions, the theoretical analysis of such problems is exceedingly difficult and no generally applicable solutions are available, except for some simple regions. Section 1 includes a discussion of some of the analytical work which has been done.

Consequently, in view of the considerable interest in dynamic fracture problems, numerical treatments of these problems are of prime importance. It is essential that reliable numerical procedures be developed which are relatively easy to use and are capable of accurately simulating dynamic crack propagation. This is by no means an easy task in view of the moving crack tip and the singularity in the stress and velocity fields at the tip itself. Section 6 considers some of the numerical techniques used in studying crack propagation problems.

The work contained in this investigation is restricted to infinitesimal deformations of homogeneous isotropic elastic bodies and to anti-plane shear displacement fields. Although of less practical interest, anti-plane shear is fundamentally simpler both analytically and numerically than plane strain, having just one non-vanishing displacement component and one characteristic wave speed. Since certain basic features of both plane and anti-plane crack propagation problems are similar, the anti-plane shear problems do yield considerable insight into crack propagation in general and may be used as a qualitative guide in analyzing the more difficult plane strain problems.

In Part I of this study, the motion of a propagating edge crack in

an elastic half-space under conditions of anti-plane shear is analyzed. An energy-balance propagation criterion is used at the crack tip to determine the velocity of the tip and an expression for the stress intensity factor at the moving crack tip is obtained.

A numerical procedure for analyzing anti-plane shear crack propagation problems using finite differences is developed in Part II. The local asymptotic displacement field near the moving crack tip is incorporated into the finite difference scheme so that in the vicinity of the crack tip, where singular stresses occur, the elastodynamic field is approximated in the numerical process as accurately as possible. The numerical scheme is applied to the edge crack problem studied in Part I and the numerical and exact results are compared.

I. THE ANALYTICAL SOLUTION OF THE EDGE CRACK PROBLEM

1. Introduction

The existing theoretical solutions to dynamic crack propagation problems have limited applicability, since they rarely include the effects of external boundaries. For non-uniform crack velocity, exact solutions of dynamic crack propagation problems—valid for all time—have only been found for simple configurations such as that of a semi-infinite crack in an otherwise unbounded body. Generally, constant velocity crack problems are more amenable to analysis and have been studied using a number of techniques. However, to determine mathematically how a plane crack propagates in a given situation, first the elastodynamic field near the crack tip has to be found for the tip moving in an arbitrary fashion in its plane and then a crack propagation criterion must be employed to find the actual motion of the tip.

The linear elastodynamic field of a propagating crack, extending non-uniformly under general anti-plane loading, was investigated by Kostrov [1] and Eshelby [2], while Freund [3] and Kostrov [4] analyzed the plane strain case. Kostrov's procedure in the anti-plane problem [1] has since been used successfully by a number of authors and is employed here. Kennedy and Achenbach [5] consider the extension of a crack which was formed by cutting at a high velocity into the surface of an elastic solid subjected to a uniform anti-plane loading. Dynamic crack growth generated by an anti-plane shear wave incident on a crack tip was investigated by Achenbach [6,7]. Molchanov and Nikitin [8], considering a finite crack propagating in an unbounded body subjected to anti-plane shear, studied the effect of the stress waves emitted from one of the moving crack tips

upon the motion of the other tip, just after the arrival of the first such wave. Recently Melville [9] examined approximately the effect of reflected stress waves on the stress intensity factor for an edge crack in anti-plane shear during crack propagation and after crack arrest. In simplifying the analysis, he assumed a constant crack tip velocity as well as a simple form for the stress distribution ahead of the initial crack tip.

2. Basic equations; energy release rate

Consider an elastic half-space containing a traction-free edge crack of initial length ℓ_0 along the x-axis (Fig. 1(a)). The deformation is assumed to be one of anti-plane shear and hence the only non-zero displacement component, which is denoted by w, is in the z-direction out of the plane of the paper in Fig. 1(a). Initially the body is in a deformed equilibrium state, with the crack tip held fixed at $x = \ell_0$. The initial static displacement field of the body in this state satisfies the boundary condition on $x = 0$ given by $w = w_0$ for $y \geqslant 0$ and $w = -w_0$ for $y \leqslant 0$, where w_0 is assumed constant. This fixed boundary condition at $x = 0$ is maintained for all time. At time $t = 0$ the crack tip is released and crack propagates along the x-axis, assuming w_0 is sufficiently large. The position of the crack tip is given by $x = \ell(t)$ at time t.

Since $w = w(x,y,t)$, the stress tensor has only two non-zero components given in terms of the displacement gradients by

$$\sigma_{zw} = \mu w_{,x} \quad \text{and} \quad \sigma_{zy} = \mu w_{,y} \quad , \tag{2.1}$$

μ being the infinitesimal shear modulus of the material. The displacement equations of motion for a homogeneous isotropic linear elastic body reduce to the wave equation

$$w_{,xx} + w_{,yy} = \frac{1}{c^2} w_{,tt} \quad , \quad c^2 = \mu/\rho \quad , \tag{2.2}$$

where ρ is the mass density and c is the shear wave speed in the body. The crack tip position $\ell(t)$ is not specified a priori but is later determined using an energy-balance propagation criterion. The only restriction imposed on $\ell(t)$ is that the crack tip velocity be less than the shear wave speed i.e. $0 \leqslant \dot{\ell}(t) < c$.

During crack propagation, the moving crack tip acts as an energy sink. As new fracture surface is being formed, the loss of mechanical energy results from the release of the internal cohesive bonds between adjoining particles in the material. The energy release rate G is defined as the amount of energy being absorbed by the moving crack tip, per unit crack tip velocity $\dot{\ell}(t)$ and per unit thickness of the crack. In general G depends upon t, $\dot{\ell}(t)$ and the crack history $\ell(r)$, $0 \le r \le t$. The flux of energy into the tip per unit time is

$$F = G\dot{\ell} \quad , \quad \dot{\ell} = \dot{\ell}(t) \quad . \tag{2.3}$$

From energy balance considerations, one has

$$F = P - \frac{d}{dt}(W + K) \quad , \tag{2.4}$$

where W and K are the strain and kinetic energies of the whole body respectively, and P represents the rate at which work is being done by the external forces on the body. Atkinson and Eshelby [10] showed

$$F = \lim_{S \to 0} \int_S \left\{ \mu \frac{\partial w}{\partial n} \frac{\partial w}{\partial t} + \dot{\ell} \left[\frac{\mu}{2} \left(\left(\frac{\partial w}{\partial x} \right)^2 + \left(\frac{\partial w}{\partial y} \right)^2 \right) + \frac{\rho}{2} \left(\frac{\partial w}{\partial t} \right)^2 \right] n_x \right\} dS \quad , \tag{2.5}$$

where S is a closed contour surrounding the crack tip and moving with it, and $\underset{\sim}{n} = (n_x, n_y)$ is the unit outward normal to S.

For a crack along the x axis with tip at $x = \ell(t)$, the dynamic anti-plane shear stress intensity factor $K_d = K_d(t)$ can be defined through

$$\sigma_{zy}(x,0,t) = (2\pi)^{-\frac{1}{2}} K_d(t) (x - \ell(t))^{-\frac{1}{2}} + O(x - \ell(t))^{\frac{1}{2}} \tag{2.6}$$

as $x \to \ell(t)$. Writing the asymptotic expressions for the stress and dis-

placement fields near the crack tip in terms of K_d , equation (2.5) with (2.3) gives (see [2])

$$G = \frac{K_d^2}{2\mu(1-\dot{\ell}^2/c^2)^{\frac{1}{2}}} \quad . \tag{2.7}$$

G as given by (2.7) will be employed in formulating the crack propagation criterion to be used for the determination of the crack history $\ell(t)$.

3. Solution of the static problem

To investigate the crack tip motion, the initial static stress field ahead of the crack is required. The configuration and boundary conditions are shown in Fig. 1(a). The crack faces are traction free, so that

$$w_{,y} = 0 \quad \text{on} \quad y = 0^{\pm} \ , \ 0 \leq x < \ell_o \qquad . \tag{3.1}$$

Since the displacement w is now time-independent, (2.2) reduces to Laplace's equation which must be solved in the right half-plane excluding the crack and subject to the appropriate boundary conditions. It is also required that w be bounded near the crack tip.

The mapping

$$\zeta = \arcsin(1 - z^2/\ell_o^2)^{\frac{1}{2}} \tag{3.2}$$

$$z = x + iy \ , \ \zeta = \xi + i\eta \ , \ (i = \sqrt{-1})$$

on taking the branch cut for $(1 - z^2/\ell_o^2)^{\frac{1}{2}}$ along the positive x axis, transforms the configuration in Fig. 1(a) onto the semi-infinite strip in Fig. 1(b) with the boundary conditions as shown. It can now be readily verified that the static displacement field $w^{st} = w^{st}(x,y)$ is

$$w^{st} = -\frac{2w_o}{\pi} \operatorname{Re}\zeta = -\frac{2w_o}{\pi} \operatorname{Re}\left\{\arcsin(1 - z^2/\ell_o^2)^{\frac{1}{2}}\right\} \qquad . \tag{3.3}$$

The stresses are found by differentiation to be given by

$$\sigma_{zx}^{st} - i\sigma_{zy}^{st} = \frac{2\mu w_o}{\pi \ell_o} (1 - z^2/\ell_o^2)^{-\frac{1}{2}} \quad . \tag{3.4}$$

Ahead of the crack tip, we have

$$\sigma_{zy}^{st}(x,0) = \mu \frac{\partial w}{\partial y}^{st}(x,0) = \frac{2\mu w_o}{\pi} (x^2 - \ell_o^2)^{-\frac{1}{2}}, \quad x > \ell_o \quad . \tag{3.5}$$

For an equilibrium crack along the x axis with tip at $x = \ell_o$, the static stress intensity factor K_{st} in anti-plane shear is defined through

$$\sigma_{zy}^{st}(x,0) = (2\pi)^{-\frac{1}{2}} K_{st} (x - \ell_o)^{-\frac{1}{2}} + O(x - \ell_o)^{\frac{1}{2}} \tag{3.6}$$

as $x \to \ell_o$, and the static energy release rate G_{st} is given by (see[11])

$$G_{st} = K_{st}^2/2\mu \quad . \tag{3.7}$$

Then using (3.5) for the edge crack under consideration, we have

$$K_{st} = \frac{2\mu w_o}{(\pi \ell_o)^{\frac{1}{2}}} \quad , \tag{3.8}$$

and

$$G_{st} = \frac{2\mu w_o^2}{\pi \ell_o} \quad . \tag{3.9}$$

4. Analysis of the dynamic problem

A. Formulation

The moving crack tip acts as a source of stress waves which propagate outward from the tip behind the cylindrical wavefront $(x - \ell_0)^2 + y^2 = (ct)^2$. Using $s = ct$ in (2.2), where c is the shear wave speed, the dynamic displacement field $w(x,y,s)$ resulting from this disturbance satisfies

$$w_{,xx} + w_{,yy} = w_{,ss} \quad . \tag{4.1}$$

Let $\bar{\ell}(s)$ denote the position of the crack tip in terms of s at time $t = s/c$, so that $\bar{\ell}(s) = \ell(s/c)$. In $\bar{\ell}(s)$, we now drop the bar for convenience and from here on, s will be used as a normalized time variable. The boundary conditions are

$$w_{,y} = 0 \quad \text{on} \quad y = 0^{\pm} \quad , \quad 0 \le x < \ell(s) \tag{4.2}$$

$$w = \begin{cases} w_0 \; ; & x = 0 \quad , \quad y > 0 \\ -w_0 \; ; & x = 0 \quad , \quad y < 0 \end{cases} \quad . \tag{4.3}$$

Initially at $s = 0$, the body is at rest i.e. $w_{,s}(x,y,0) \equiv 0$ and the initial static displacement $w = w^{st}(x,y)$ is given in (3.3).

Let $w'(x,y,s) = w(x,y,s) - w^{st}(x,y)$ denote the change in displacement from the initial static configuration. The boundary condition at $x = 0$ now becomes $w'(0,y,s) \equiv 0$. As a consequence of this fixed end condition at $x = 0$, the reflected stress waves must be equal in magnitude but opposite in sign to the incident waves at this location. To incorporate the effect of these reflected waves, we consider a center crack in an infinite body with tips at $x = \pm\ell(s)$ i.e. moving at the same rate but in

opposite directions. Then the residual displacement w' must satisfy the two-dimensional wave equation (4.1) in the full (x,y) - plane excluding the crack, with zero initial conditions and the boundary conditions on the crack surfaces are given by

$$\mu \frac{\partial w'}{\partial y}(x,0^{\pm}s) = \begin{cases} 0, & 0 \le x < \ell_0 \\ -P(x), & \ell_0 < x < \ell(s) \end{cases} , \tag{4.4}$$

$$\mu \frac{\partial w'}{\partial y}(x,0^{\pm},s) = \begin{cases} 0, & -\ell_0 < x \le 0 \\ P(-x), & -\ell(s) < x < -\ell_0 \end{cases} , \tag{4.5}$$

where, from equation (3.5), $P(x)$ is given by

$$P(x) = \sigma_{zy}^{st}(x,0) = \frac{2\mu w_0}{\pi}(x^2 - \ell_0^2)^{-\frac{1}{2}}, \quad x > \ell_0 \ . \tag{4.6}$$

The solution satisfies $w'(0,y,s) \equiv 0$ as required. Hence the half-plane problem with the edge crack under consideration is equivalent to the full-plane problem with a center crack as described above.

B. Green's Function method

Since the initial static displacement field $\overline{w}(x,y)$ is anti-symmetric in y, $w(x,y,s)$ and hence $w'(x,y,s)$ is also anti-symmetric in y. In what follows, only the half-plane $y \ge 0$ is considered. Kostrov's method of solution [1], employed here, uses the Green's Function G which satisfies the two-dimensional wave equation (4.1) in the half-plane $y \ge 0$, with zero initial conditions and the boundary condition

$$\sigma_{zy}(x,0,s) = \mu \frac{\partial G}{\partial y}(x,0,s) = \delta(x - x_0)\delta(s - s_0) \quad , \tag{4.7}$$

where $-\infty < x_0 < \infty$ and $0 \le s_0 < s$. The displacement wave generated by this impulsive load is (see [13])

$$G(x - x_0, y, s - s_0) = - \frac{1}{\pi\mu R} H\{(s - s_0) - [(x - x_0)^2 + y^2]^{\frac{1}{2}}\} \quad , \tag{4.8}$$

where $H\{\ \}$ is the Heaviside step function and R is given by

$$R = \{(s - s_0)^2 - (x - x_0)^2 - y^2\}^{\frac{1}{2}} \quad . \tag{4.9}$$

This is a cylindrical wave emanating from the line $x = x_0$, $y = 0$ for $s > s_0$.

For general boundary conditions of the form

$$\sigma_{zy}(x,0,s) = \sigma(x,s) \quad , \tag{4.10}$$

linear superposition gives

$$w'(x,y,s) = - \frac{1}{\pi\mu} \iint_A \frac{\sigma(x_0,s_0)}{R} dx_0 ds_0 \quad , \tag{4.11}$$

where R is given in (4.9) and the region of integration A is the parabolic region in the $x_0 - s_0$ plane satisfying

$$s - s_0 - [(x - x_0)^2 + y^2]^{\frac{1}{2}} \ge 0 \quad , \quad s > s_0 \ge 0 \quad . \tag{4.12}$$

On $y = 0$, A reduces to a triangular region. Introducing the characteristic coordinates

$$\xi = (s - x)/\sqrt{2} \quad \text{and} \quad \eta = (s + x)/\sqrt{2} \quad , \tag{4.13}$$

the expression for R in (4.9), on setting $y = 0$, simplifies to

$$R = \sqrt{2}(\xi - \xi_0)^{\frac{1}{2}}(\eta - \eta_0)^{\frac{1}{2}} \quad . \tag{4.14}$$

From (4.11), the displacement $w'(x,0,s) \equiv w'(\xi,\eta)$, on using (4.14), becomes

$$w'(\xi\ \eta) = -\frac{1}{\pi\mu\sqrt{2}} \int \frac{d\xi_0}{(\xi - \xi_0)^{\frac{1}{2}}} \int \frac{\sigma(\xi_0,\eta_0)d\eta_0}{(\eta - \eta_0)^{\frac{1}{2}}} \quad . \tag{4.15}$$

The (x,s)-diagram is shown in Fig. 2, along with the crack tip trajectories and wavefronts. To determine the motion of the crack tip, the energy release rate and hence the stress intensity factor at the tip must be found.

C. The field before the arrival of the first reflected wave

The first reflected stress wave strikes the crack tip at $s = s_r$, where s_r satisfies

$$\ell(s_r) + \ell_0 = s_r \quad . \tag{4.16}$$

From [2], or following the approach used in [12], the shear stress ahead of the crack tip before the arrival of the first reflected stress wave is

$$\sigma_1(x,s) = \frac{(1 - \ell'(s))^{\frac{1}{2}}}{\pi(x - \ell(s))^{\frac{1}{2}}} I_0(s) + O(x - \ell(s))^{\frac{1}{2}} \quad , \tag{4.17}$$

where

$$I_o(s) = \int_{\ell_o}^{\ell(s)} \frac{P(v)dv}{(\ell(s) - v)^{\frac{1}{2}}} \quad . \tag{4.18}$$

Evaluating I_o, where $P(v) = \sigma_{zy}^{st}(v,0)$ is obtained from (3.5), gives

$$I_o = \frac{4\mu w_o}{\pi} \frac{K(k)}{(\ell + \ell_o)^{\frac{1}{2}}} \quad , \quad k = \left(\frac{\ell - \ell_o}{\ell + \ell_o} \right)^{\frac{1}{2}} \quad . \tag{4.19}$$

Here $K(k)$ is the complete elliptic integral of the first kind. The stress intensity factor then is

$$K_d(s) = (2/\pi)^{\frac{1}{2}}(1-\ell'(s))^{\frac{1}{2}} I_o(s) \quad , \quad 0 \le s < s_r \tag{4.20}$$

and the energy release rate at the crack tip is

$$G(s) = \frac{1}{\pi\mu} \left(\frac{1 - \ell'(s)}{1 + \ell'(s)} \right)^{\frac{1}{2}} I_o(s)^2 \quad , \quad 0 \le s < s_r \quad . \tag{4.21}$$

D. The field after the arrival of the first reflected wave

After the first reflected stress wave strikes the moving crack tip at the instant $s = s_r$ given by (4.16), a diffracted wave is emitted. This diffracted wave propagates outward behind a cylindrical wavefront with the shear wave speed, hits the fixed boundary at $x = 0$ and is reflected. It strikes the crack tip again at $s = s_d$, where from Fig. 2, s_d satisfies

$$s_d - \ell(s_d) = s_r + \ell(s_r) \quad . \tag{4.22}$$

We now analyze the stress field in the crack plane near the tip for $s_r < s < s_d$.

In terms of ξ and η , the crack tip trajectory $x = \ell(s)$ becomes $\eta = L(\xi)$ where $L(\xi)$ satisfies

$$\frac{L(\xi) - \xi}{\sqrt{2}} = \ell\left(\frac{L(\xi) + \xi}{\sqrt{2}}\right) \quad . \tag{4.23}$$

Similarly $x = -\ell(s)$ becomes $\eta = \tilde{L}(\xi)$ where

$$\frac{\tilde{L}(\xi) - \xi}{\sqrt{2}} = -\ell\left(\frac{\tilde{L}(\xi) + \xi}{\sqrt{2}}\right) \quad . \tag{4.24}$$

The initial crack tip locations $x = \pm\ell_o$ are denoted by $\eta = \eta_\pm(\xi) = \xi \pm \sqrt{2}\,\ell_o$.

Consider the point with characteristic coordinates (ξ_2, η_2) shown in Fig. 2, where for $\xi_r = \ell_o/\sqrt{2}$,

$$\xi_r < \xi_2 < \xi_d \quad \text{and} \quad \eta_2 > L(\xi_2) \quad . \tag{4.25}$$

Here $\xi_d = (s_d - \ell(s_d))/\sqrt{2}$ is the value of ξ when the diffracted wave meets the right crack tip at $s = s_d$ and $x = \ell(s_d)$. The domain of dependence is below the dotted lines shown. We denote by $\sigma_1(\xi,\eta)$ the shear stress σ_{zy} at the point (ξ,η) ahead of the right crack tip for $-\xi_r < \xi < \xi_r$ and similarly let $\tilde{\sigma}_1(\xi,\eta)$ represent the shear stress σ_{zy} ahead of the left crack tip for $-\eta_r < \eta < \eta_r$, where $\eta_r = \ell_o/\sqrt{2}$. The change in displacement $w'(\xi_2,\eta_2)$ ahead of the right crack tip is zero giving, from (4.15)

$$\int_{-\xi_r}^{\xi_2}\int_{\eta_+(\xi)}^{L(\xi)} \frac{P(\xi,\eta)}{R}d\eta d\xi - \int_{-\xi_r}^{\xi_r}\int_{L(\xi)}^{\eta_2} \frac{\sigma_1(\xi,\eta)}{R}\, d\eta d\xi - \int_{\xi_r}^{\xi_2}\int_{L(\xi)}^{\eta_2} \frac{\sigma_2(\xi,\eta)}{R}\, d\eta d\xi$$

$$+ \int_{\xi_r}^{\xi_2}\int_{\tilde{L}(\xi)}^{\eta_-(\xi)} \frac{\tilde{P}(\xi,\eta)}{R}\, d\eta d\xi - \int_{\xi_r}^{\xi_2}\int_{-\eta_r}^{\tilde{L}(\xi)} \frac{\tilde{\sigma}_1(\xi,\eta)}{R}\, d\eta d\xi = 0 \quad . \tag{4.26}$$

Here R is given in (4.14),

$$P(\xi,\eta) = P((\eta - \xi)/\sqrt{2}) = P(x) \tag{4.27}$$

and

$$\tilde{P}(\xi,\eta) = \tilde{P}((\eta - \xi)/\sqrt{2}) = \tilde{P}(x) = -P(-x) \quad . \tag{4.28}$$

At (ξ_1,η_1) in Fig. 2, where $-\xi_r < \xi_1 < \xi_r$ and $\eta_1 > L(\xi_1)$, that is before the arrival of the first reflected wave, $w'(\xi_1,\eta_1)$ is also zero, giving

$$\int_{-\xi_r}^{\xi_1}\int_{\eta_+(\xi)}^{L(\xi)} \frac{P(\xi,\eta)}{R}\, d\eta d\xi - \int_{-\xi_r}^{\xi_1}\int_{L(\xi)}^{\eta_1} \frac{\sigma_1(\xi,\eta)}{R}\, d\eta d\xi = 0 \quad . \tag{4.29}$$

Extending the definition of $\sigma_1(\xi,\eta)$ to the region $\xi_r < \xi < \xi_2$ and $\eta > L(\xi)$, where $\sigma_1(\xi,\eta)$ is here taken as the shear stress at (ξ,η) if the first reflected stress wave is not taken into account, then the second term of (4.26) can be rewritten as

$$\int_{-\xi_r}^{\xi_r}\int_{L(\xi)}^{\eta_2} \frac{\sigma_1(\xi,\eta)}{R}\,d\eta d\xi = \int_{-\xi_r}^{\xi_2}\int_{L(\xi)}^{\eta_2} \frac{\sigma_1(\xi,\eta)}{R}\,d\eta d\xi - \int_{\xi_r}^{\xi_2}\int_{L(\xi)}^{\eta_2} \frac{\sigma_1(\xi,\eta)}{R}\,d\eta d\xi \quad . \quad (4.30)$$

By virtue of (4.29) with (ξ_1,η_1) replaced by (ξ_2,η_2) and (4.30), equation (4.26) on using (4.14) becomes

$$\int_{\xi_r}^{\xi_2} \frac{d\xi}{(\xi_2-\xi)^{\frac{1}{2}}} \int_{L(\xi)}^{\eta_2} \frac{[\sigma_2(\xi,\eta)-\sigma_1(\xi,\eta)]d\eta}{(\eta_2-\eta)^{\frac{1}{2}}}$$

$$= \int_{\xi_r}^{\xi_2} \frac{d\xi}{(\xi_2-\xi)^{\frac{1}{2}}} \int_{\tilde{L}(\xi)}^{\eta_-(\xi)} \frac{\tilde{P}(\xi,\eta)d\eta}{(\eta_2-\eta)^{\frac{1}{2}}} - \int_{\xi_r}^{\xi_2} \frac{d\xi}{(\xi_2-\xi)^{\frac{1}{2}}} \int_{-\eta_r}^{\tilde{L}(\xi)} \frac{\tilde{\sigma}_1(\xi,\eta)d\eta}{(\eta_2-\eta)^{\frac{1}{2}}} \quad . \quad (4.31)$$

Equation (4.31) is clearly satisfied by

$$\int_{L(\xi)}^{\eta_2} \frac{[\sigma_2(\xi,\eta)-\sigma_1(\xi,\eta)]d\eta}{(\eta_2-\eta)^{\frac{1}{2}}} = \int_{\tilde{L}(\xi)}^{\eta_-(\xi)} \frac{\tilde{P}(\xi,\eta)d\eta}{(\eta_2-\eta)^{\frac{1}{2}}} - \int_{-\eta_r}^{\tilde{L}(\xi)} \frac{\tilde{\sigma}_1(\xi,\eta)d\eta}{(\eta_2-\eta)^{\frac{1}{2}}} \quad . \quad (4.32)$$

This is an integral equation for $\sigma_2(\xi,\eta) - \sigma_1(\xi,\eta)$ of the Abel kind which can be solved analytically to give

$$\sigma_2(\xi,\eta) - \sigma_1(\xi,\eta) = \frac{1}{\pi(\eta-L(\xi))^{\frac{1}{2}}}\left\{\int_{\tilde{L}(\xi)}^{\eta_-(\xi)} \frac{\tilde{P}(\xi,u)[L(\xi)-u]^{\frac{1}{2}}}{\eta-u}\,du - \int_{\eta_r}^{\tilde{L}(\xi)} \frac{\tilde{\sigma}_1(\xi,u)[L(\xi)-u]^{\frac{1}{2}}}{\eta-u}\,du\right\} \quad . \tag{4.33}$$

Similarly from (4.29) with (ξ_1,η_1) replaced by (ξ_2,η_2), it follows that

$$\int_{L(\xi)}^{\eta_2} \frac{\sigma_1(\xi,\eta)}{(\eta_2-\eta)^{\frac{1}{2}}}\,d\eta = \int_{\eta_+(\xi)}^{L(\xi)} \frac{P(\xi,\eta)}{(\eta_2-\eta)^{\frac{1}{2}}}\,d\eta \quad , \tag{4.34}$$

which upon solving gives

$$\sigma_1(\xi,\eta) = \frac{1}{\pi(\eta-L(\xi))^{\frac{1}{2}}} \int_{\eta_+(\xi)}^{L(\xi)} \frac{P(\xi,u)[L(\xi)-u]^{\frac{1}{2}}}{\eta-u}\,du \quad . \tag{4.35}$$

Combining (4.33) and (4.35) gives the change in shear stress ahead of the right crack tip, taking the first reflected stress wave into account i.e.

$$\sigma_2(\xi,\eta) = \frac{1}{\pi(\eta-L(\xi))^{\frac{1}{2}}}\left\{\int_{\eta_+(\xi)}^{L(\xi)} \frac{P(\xi,u)[L(\xi)-u]^{\frac{1}{2}}}{\eta-u}\,du + \int_{\tilde{L}(\xi)}^{\eta_-(\xi)} \frac{\tilde{P}(\xi,u)[L(\xi)-u]^{\frac{1}{2}}}{\eta-u}\,du - \int_{-\eta_r}^{\tilde{L}(\xi)} \frac{\tilde{\sigma}_1(\xi,u)[L(\xi)-u]^{\frac{1}{2}}}{\eta-u}\,du\right\} \quad . \tag{4.36}$$

To express $\sigma_2(\xi,\eta)$ in terms of the physical variables x and s, we introduce new parameters

$$\bar{s} = \frac{L(\xi)+\xi}{\sqrt{2}} \quad \text{and} \quad \bar{s}_2 = \frac{\tilde{L}(\xi)+\xi}{\sqrt{2}} \quad . \tag{4.37}$$

Using (4.23), one finds that $\bar{s}$ satisfies

$$\bar{s} - \ell(\bar{s}) = s - x \tag{4.38}$$

and from (4.24)

$$\bar{s}_2 + \ell(\bar{s}_2) = s - x \quad . \tag{4.39}$$

Introducing $\bar{s}$ and $\bar{s}_2$ defined in (4.37) and the substitution $v = (u-\xi)/\sqrt{2}$, (4.36) becomes

$$\sigma_2(x,s) = \frac{1}{\pi(x-\ell(\bar{s}))^{\frac{1}{2}}} \left\{ \int_{\ell_0}^{\ell(\bar{s})} \frac{P(v)[\ell(\bar{s})-v]^{\frac{1}{2}}}{x-v}\,dv + \int_{-\ell(\bar{s}_2)}^{-\ell_0} \frac{\tilde{P}(v)[\ell(\bar{s})-v]^{\frac{1}{2}}}{x-v}\,dv \right.$$

$$\left. - \int_{\beta_1(x,s)}^{-\ell(\bar{s}_2)} \frac{\tilde{\sigma}_1(v,s-x+v)[\ell(\bar{s})-v]^{\frac{1}{2}}}{x-v}\,dv \right\} , \tag{4.40}$$

where

$$\beta_1(x,s) = -(x-s-\ell_0)/2 \quad . \tag{4.41}$$

To find the stress intensity factor, the asymptotic behavior of (4.40) for $0 < x - \ell(s) \ll 1$ must be examined. For $x = \ell(s)$, (4.38) is satisfied by $\bar{s} = s$. Expanding about $x = \ell(s)$ using (4.38), gives

$$\bar{s}(x,s) = s - (1 - \ell'(s))^{-1}(x-\ell(s)) + O(x - \ell(s))^2 \quad , \tag{4.42}$$

whence $\ell(\bar{s}) = \ell(s) + O(x - \ell(s))$. From (4.41) $\beta_1(x,s) = \bar{\beta}(s) + O(x - \ell(s))$, where

$$\bar{\beta}(s) = - (\ell(s) - s - \ell_0)/2 \quad . \tag{4.43}$$

Equation (4.39) may be rewritten as

$$\bar{s}_2 + \ell(\bar{s}_2) = s - \ell(s) - (x - \ell(s)) \quad . \tag{4.44}$$

Let s_2 be the solution of

$$s_2 + \ell(s_2) = s - \ell(s) \quad . \tag{4.45}$$

For $s_r \le s < s_d$, one can show that $0 \le s_2 < s_r$. From (4.44), $\bar{s}_2 = s_2 + O(x-\ell(s))$ and so $\ell(\bar{s}_2) = \ell(s_2) + O(x-\ell(s))$. Physically, the stress wave arriving at the right crack tip $x = \ell(s)$ at time $t = s/c$ was emitted at the left crack tip $x = -\ell(s_2)$ at time $t_2 = s_2/c$. Using the above asymptotic results for $\bar{s}$ and $\bar{s}_2$ near $x = \ell(s)$, equation (4.40), after some further manipulation, becomes

$$\sigma_2(x,s) = \frac{(1 - \ell'(s))^{\frac{1}{2}}}{\pi(x - \ell(s))^{\frac{1}{2}}} I_r(s) + O(x - \ell(s))^{\frac{1}{2}} \quad , \tag{4.46}$$

where

$$I_r(s) = \int_{\ell_o}^{\ell(s)} \frac{P(v)dv}{(\ell(s)-v)^{\frac{1}{2}}} + \int_{-\ell(s_2)}^{-\ell_o} \frac{\tilde{P}(v)dv}{(\ell(s)-v)^{\frac{1}{2}}} - \int_{-\bar{\beta}(s)}^{-\ell(s_2)} \frac{\tilde{\sigma}_1(v,s-\ell(s)+v)dv}{(\ell(s)-v)^{\frac{1}{2}}} \quad . \quad (4.47)$$

Here $\bar{\beta}(s)$ is given by (4.43) and s_2 satisfies (4.45).

In (4.47), $\tilde{\sigma}_1(x,s)$ the shear stress ahead of the left crack tip for $0 \le s < s_r$ is required. Equation (4.35) gives $\sigma_1(\xi,\eta)$, the shear stress ahead of the right crack tip before the first reflected wave arrives. Transforming $\sigma_1(\xi,\eta)$ to the variables x and s as was done for $\sigma_2(\xi,\eta)$ gives

$$\sigma_1(x,s) = \frac{1}{\pi(x-\ell(\bar{s}))^{\frac{1}{2}}} \int_{\ell_o}^{\ell(\bar{s})} \frac{P(v)[\ell(\bar{s})-v]^{\frac{1}{2}}}{x-v}\, dv \quad , \quad (4.48)$$

where $\bar{s}$ is given by (4.38). By virtue of the symmetry in the problem, replacing x by $-x$, v by $-v_1$ and $P(v)$ by $-P(-v_1)$ in the integrand of (4.48) gives $\tilde{\sigma}_1(x,s)$, the shear stress ahead of the left crack tip for $0 \le s < s_r$, i.e.

$$\tilde{\sigma}_1(x,s) = \frac{1}{\pi(-x-\ell(s_1))^{\frac{1}{2}}} \int_{-\ell_o}^{-\ell(s_1)} \frac{\tilde{P}(v_1)[\ell(s_1)+v_1]^{\frac{1}{2}}}{x-v_1}\, dv_1 \quad (4.49)$$

in which $\tilde{P}(v_1) = -P(-v_1)$ and s_1 satisfies

$$s_1 - \ell(s_1) = s + x \quad . \quad (4.50)$$

Equation (4.49) now yields

$$\tilde{\sigma}_1(v,s-\ell(s)+v) = -\frac{1}{\pi(-v-\ell(\tilde{s}_1))^{\frac{1}{2}}} \int_{-\ell(\tilde{s}_1)}^{-\ell_o} \frac{\tilde{P}(v_1)[\ell(\tilde{s}_1)+v_1]^{\frac{1}{2}}}{v-v_1}\, dv_1 \ , \qquad (4.51)$$

where from (4.50), $\tilde{s}_1$ is obtained from the relation

$$\tilde{s}_1 - \ell(\tilde{s}_1) = s - \ell(s) + 2v \ . \qquad (4.52)$$

For $s_r \le s < s_d$, one can show $0 \le s_2 < s_r$ and $0 \le \tilde{s}_1 < s_2$. Evaluating the integral in (4.51), one gets

$$\tilde{\sigma}_1(v,s-\ell(s)+v) = -\frac{4w_o\mu}{\pi^2} \frac{[K(\tilde{k})-\Pi(\tilde{\alpha},\tilde{k})]}{(\ell(\tilde{s}_1)+\ell_o)^{\frac{1}{2}}(-v-\ell(\tilde{s}_1))^{\frac{1}{2}}} \ , \qquad (4.53)$$

where

$$\tilde{k}^2 = \tilde{k}(\tilde{s}_1)^2 = \frac{\ell(\tilde{s}_1)-\ell_o}{\ell(\tilde{s}_1)+\ell_o} \quad \text{and} \quad \tilde{\alpha} = \tilde{\alpha}(\tilde{s}_1,v) = \frac{\ell(\tilde{s}_1)-\ell_o}{\ell(\tilde{s}_1)+v} \ . \qquad (4.54)$$

Here $\Pi(\tilde{\alpha},\tilde{k})$ is the complete elliptic integral of the third kind. Note that $\tilde{\alpha} \le 0$ for all v in the interval $(-\bar{\beta}(s), -\ell(s_2))$. The second term of (4.47), on performing the integration, is

$$\int_{-\ell(s_2)}^{-\ell_o} \frac{\tilde{P}(v)dv}{(\ell(s)-v)^{\frac{1}{2}}} = -\frac{4w_o\mu}{\pi} \frac{F(\varphi,k)}{(\ell(s)+\ell_o)^{\frac{1}{2}}} \ . \qquad (4.55)$$

In (4.55) $F(\varphi,k)$ is the incomplete elliptic integral of the first kind,

where $k = k(s)$ is given in (4.19) and

$$\varphi = \varphi(s_2) = \arcsin\left(\frac{\ell(s_2)-\ell_0}{\ell(s_2)+\ell_0}\right)^{\frac{1}{2}} \quad . \tag{4.56}$$

Letting

$$\tilde{I}(s) = \frac{\pi(2\ell_0)^{\frac{1}{2}}}{4\mu w_0} I_r(s) \quad ,$$

and using (4.19), (4.53) and (4.55), equation (4.47) becomes

$$\tilde{I}(s) = (1-k^2)^{\frac{1}{2}}(K(k)-F(\varphi,k))$$

$$+ \frac{(2\ell_0)^{\frac{1}{2}}}{\pi} \int_{-\bar{\beta}(s)}^{-\ell(s_2)} \frac{[K(\tilde{k})-\Pi(\tilde{\alpha},\tilde{k})]dv}{(-\ell(\tilde{s}_1)-v)^{\frac{1}{2}}\,(\ell(\tilde{s}_1)+\ell_0)^{\frac{1}{2}}(\ell(s)-v)^{\frac{1}{2}}} \quad . \tag{4.57}$$

Here $k = k(s)$ and $\varphi = \varphi(s_2)$ are given in (4.19) and (4.56) resp., while $\tilde{k} = \tilde{k}(\tilde{s}_1)$ and $\tilde{\alpha} = \tilde{\alpha}(\tilde{s}_1, v)$ are given in (4.54). By virtue of (2.6), the stress intensity factor then is

$$K_d(s) = \frac{4\mu w_0}{\pi^{\frac{3}{2}}\ell_0^{\frac{1}{2}}}(1-\ell'(s))^{\frac{1}{2}}\,\tilde{I}(s) \quad ; \quad s_r \le s < s_d \tag{4.58}$$

and from (2.7), it follows that the energy release rate at the right crack tip is

$$G(s) = \frac{8\mu w_0^2}{\pi^3 \ell_0}\left(\frac{1-\ell'(s)}{1+\ell'(s)}\right)^{\frac{1}{2}}\tilde{I}(s)^2 \quad , \quad s_r \le s < s_d \quad . \tag{4.59}$$

5. Motion of the crack tip

During the fracture process, the moving crack tip absorbs energy from the surrounding material. According to prevailing views of fracture, the energy absorbed by the tip is used to create the new free surface generated by crack propagation. In the usual quantitative model of this process, one postulates the existence of a "specific fracture energy" Γ which is characteristic of the material at hand and which has the property that, during crack propagation, the relation

$$G = \Gamma \tag{5.1}$$

holds at every instant. According to (4.21), (4.19) and (4.59), (4.57), G depends on the crack length history $\ell(r)$, $0 \le r \le s$ and on the instantaneous crack tip velocity $\ell'(s)$. In general Γ may be a (given) function of $\ell'(s)$; we consider only the simplest model, in which Γ is an absolute constant. Equation (5.1) with Γ = constant is thus our crack propagation criterion. It may be regarded as an "equation of motion" for the crack tip.

In Section 2, it was assumed that the crack tip was held fixed until time $t = 0$, when it is released and the crack propagation process begins. For propagation to occur at all, (5.1) requires that the static energy release rate G_{st} satisfy $G_{st} > \Gamma$. Thus by (3.9), one must have

$$\frac{2\mu w_o^2}{\pi \ell_o} > \Gamma \quad . \tag{5.2}$$

A dimensionless parameter Q is now introduced through

$$Q = \frac{2\mu w_o^2}{\pi \ell_o \Gamma} \quad . \tag{5.3}$$

Then for crack extension to occur, from (5.2) it is necessary that Q be larger than unity.

Before the arrival of the first reflected stress wave, the crack tip equation of motion is, by (4.21), (4.19) and (5.1),

$$\frac{16 w_o^2 \mu}{\pi^3} \left(\frac{1-\ell'(s)}{1+\ell'(s)}\right)^{\frac{1}{2}} \frac{K(k)^2}{(\ell(s)+\ell_o)} = \Gamma \quad . \tag{5.4}$$

Using (5.3) and the definition of $k = k(\ell(s))$ in (4.19), the differential equation in (5.4), on solving for $\ell'(s)$, becomes

$$\ell'(s) = \frac{K(k)^4(1-k^2)^2 - \pi^4/16Q^2}{K(k)^4(1-k^2)^2 + \pi^4/16Q^2} \quad , \quad 0 \le s < s_r \quad . \tag{5.5}$$

At $s = 0$, we have $k = 0$ and $K(0) = \pi/2$ giving

$$\ell'(0) = \frac{Q^2 - 1}{Q^2 + 1} \quad . \tag{5.6}$$

Since $Q > 1$ is necessary for crack extension to occur, $\ell'(0)$ must be positive. Because $k = k(\ell(s))$, equation (5.5) is an autonomous differential equation for ℓ with a critical point at $k = k_r$, where

$$K(k_r)^2(1 - k_r^2) = \pi^2/4Q \quad . \tag{5.7}$$

Since an infinite amount of time is required to reach a critical point, the crack cannot arrest before the arrival of the first reflected stress wave. At $s = s_r$, for $Q > 1$ the crack tip is moving with non-zero velocity $\ell'(s_r)$ where $0 < \ell'(s_r) < 1$.

After the arrival of the first reflected wave at $s = s_r$ until the arrival of the second reflected wave at $s = s_d$, from (4.59) and (5.1), the equation governing the crack tip motion is

$$\frac{8\mu w_o^2}{\pi^3 \ell_o} \left(\frac{1-\ell'(s)}{1+\ell'(s)} \right)^{\frac{1}{2}} \tilde{I}(s)^2 = \Gamma \quad . \tag{5.8}$$

Here $\tilde{I}(s)$ is given by (4.57). Using (5.3), this equation reduces to solving

$$\ell'(s) = \frac{\tilde{I}(s)^4 - \pi^4/16Q^2}{\tilde{I}(s)^4 + \pi^4/16Q^2} \quad , \quad s_r \leq s < s_d \quad , \tag{5.9}$$

where $\ell(s_r)$ is obtained from the solution of (5.5). From (4.57), $\tilde{I}(s)$ depends upon the instantaneous variables s and $\ell(s)$, and upon the delayed crack length $\ell(s_2)$. If for some value of s in the interval (s_r, s_d)

$$\tilde{I}(s)^2 - \pi^2/4Q = 0 \quad , \tag{5.10}$$

then $\ell'(s) = 0$ and the crack arrests. Given values of ℓ_o and Q, numerical solutions of (5.5) and (5.9) can be obtained, with the value of s_r being determined from (4.16). The results of these investigations have shown that crack arrest does indeed occur in the time interval

(s_r, s_d). However due to the complicated nature of $\tilde{I}(s)$, it is unclear whether arrest always takes place in the interval (s_r, s_d), particularly for very large Q.

If in the original formulation of the problem, the variables x, y, s and w are made dimensionless by considering instead x/ℓ_o, y/ℓ_o, s/ℓ_o and w/w_o, then the governing differential equation (4.1) and the initial and boundary conditions (3.3), (4.2), (4.3) are independent of all parameters appearing in the problem. In the failure criterion, from (2.3), (2.5) and (5.1), the only variable parameter appearing is Q, defined in (5.3). In Fig. 3, the normalized crack tip velocity $\ell'(s)$ is plotted against s/ℓ_o for $Q = 1.5$ and crack arrest occurs before the second reflected wave reaches the tip. Similar results were obtained for other values of Q, both larger and smaller that $Q = 1.5$.

In Fig. 4 the dynamic stress intensity factor $K_d(s)$, normalized by its initial static value K_{st} given in (3.8), is shown plotted against s/ℓ_o, $0 \le s \le s_d$, again for $Q = 1.5$. $K_d(s)$ drops discontinuously at $s = 0$ from its initial static value and then increases due to decreasing crack velocity up to arrest. After arrest occurs, the stress intensity factor decreases until the arrival of the next reflected stress wave at $s = s_d$. The effect of this stress wave arriving at $s = s_d$ is to reduce the rate at which the stress intensity factor is decreasing and possibly even to begin increasing it after some time. The effects of the succeeding reflected stress waves upon the stress intensity factor become increasingly more difficult to analyze by this method. We have not attempted such an analysis.

II. THE NUMERICAL SOLUTION OF THE EDGE CRACK PROBLEM

6. Introduction

In this section we discuss some of the techniques which have been used as well as the difficulties associated with the numerical solution of rapidly moving crack problems. For given initial and boundary conditions, numerical studies of dynamic crack propagation problems are generally conducted in one of two different ways. First, given the crack tip position or velocity history which may have been experimentally observed or is simply prescribed, then by forcing the numerical model to respond in exactly the same manner, one can calculate items of interest such as the dynamic stress intensity factor at the tip or possibly use the model to study material properties from laboratory tests. Alternatively, given a failure criterion as in (5.1), one can compute the resulting crack growth history and the crack arrest point if arrest occurs. This may be used to study the integrity of a structural component.

Most of the existing numerical work done in simulating two-dimensional crack propagation in linear elastic bodies has been performed by either the finite difference or the finite element method. In a critical review of numerical solution techniques in dynamic fracture mechanics [14] in 1978, Kanninen discussed some of the deficiencies inherent in both methods and stated that "Currently, finite elements are better suited for initiation of growth calculations while finite differences can better cope with crack propagation and arrest". Since then further contributions have been made to both of these methods with particular emphasis on representing the motion of the crack tip and the singular stress field locally near the tip as accurately as possible. We now briefly review some of the work

which has been done.

In the finite element method, the modeling of crack propagation problems using conventional elements everywhere has been found to be not sufficiently accurate [14]. Taking advantage of special elements near the tip which incorporate the characteristic linear elastic crack tip singularity in the stress field, the finite element method has been applied successfully to equilibrium crack problems [15] and to crack growth initiation problems [16]. Incorporating the singular element idea at a moving tip in a propagating crack problem has been somewhat more difficult. The particular choice of singular element used can be very important and also the advancement of the tip by sudden node release can be a source of large transient oscillations in the numerical model [17,18].

Aoki et al [19,20] use a singular element incorporating the lowest order asymptotic displacement eigenfunction at the moving crack tip and as the tip gets close to the boundary of this singular element, the entire element is shifted as a rigid body to a new location. Nishioka and Atluri [21,22] use a linear combination of crack tip displacement eigenfunctions valid for a constant velocity tip to construct a singular crack tip element and in the numerical scheme this element moves with the tip at each time step being surrounded by deforming regular finite elements. The details involved however are somewhat elaborate. The above two sets of authors apply their numerical schemes to problems involving prescribed crack velocity [19,21] and also to cases where a failure criterion is given and the crack velocity history is to be determined [20,22]. Their results correlate reasonably well with analytical solutions where such a comparison can be made.

The finite difference scheme models crack growth by expressing the elastodynamic equations of motion in difference form at each node point of a finite grid covering the body. In the earlier models [23,24,25], crack growth is simulated by intermittent crack extensions of magnitude one mesh size which implies the solution of a sequence of transient problems, each contributing to a disturbing numerical noise with no physical counterpart. In [25] a transition zone is used at the moving tip to aid in remedying the above difficulty. Because of the discontinuous nature of the crack motion and the inadequate representation of the local stress and displacement fields near the moving tip, the degree of resolution and accuracy obtained in the numerical results from these models is not sufficiently good for extensive investigations.

To improve the local accuracy at the moving tip and in particular to overcome the problem of intermittent crack extension, Aboudi[26] transforms the equations of motion to a moving coordinate system with origin at the moving crack tip. A finite difference scheme involving the crack tip velocity and acceleration is developed for both the plane strain and anti-plane shear cases and is applied to a number of problems with prescribed crack history. Shmuely and Perl [27,28] introduce in the vicinity of the propagating crack tip a local moving grid which moves with the velocity of the tip and has its origin of coordinates at the moving tip. Outside of the moving grid, a stationary grid is used which readily accommodates the boundary conditions for finite specimens. Separate difference schemes are established governing the motion in both the moving and stationary domains. As in the model by Aboudi, the difference scheme for the moving domain directly involves the crack tip velocity and

acceleration, and the method is applied to a number of problems also with prescribed crack history. In the prediction case of crack growth embodying a failure criterion, the objective is the determination of the crack tip position and velocity. Finding the crack tip acceleration is an order of magnitude more difficult and requires that the velocity of the tip be evaluated with a high degree of accuracy and resolution. Hence because the acceleration and velocity of the tip occur explicitly in both of the above difference schemes, they are not totally suitable for the determination of crack growth history.

Unlike the situation in the finite element case, little effort has been made in finite difference simulations to incorporate the asymptotic nature of the stress and displacement fields near the moving crack tip. In not doing so, the singular stress field near the tip is smoothed out, thereby affecting the numerical solution and special care is needed in finding the stress intensity factor. Burgers [29] uses one term asymptotic expansions about the crack tip position to approximate the stresses and particle velocity in the region near the tip of a propagating crack in anti-plane shear. The difference equations are given in terms of the three displacement gradients and are obtained on integrating the equations of motion along bicharacteristic strips. The stress intensity factor is computed for both steady and unsteady prescribed crack tip velocities and compared with known values. The results are reasonably accurate for steady crack propagation but fairly large errors occur for the unsteady propagation cases.

In the following sections, we model dynamic crack propagation under anti-plane shear using an explicit finite difference scheme derived from

the displacement equation of motion. To improve the local accuracy near the moving crack tip at which singular stresses occur and to smoothly extend the crack at each time step, the lowest order asymptotic displacement term near the tip is used in conjunction with the finite difference scheme to simulate the problem as accurately as possible. The procedure is applied to the edge crack problem discussed in Sections 2,3 and 4, finding the crack tip velocity and the dynamic stress intensity factor numerically. To check the accuracy of the method, the numerical and analytical results are compared.

7. The displacement field near the moving crack tip

This section deals with determining the behavior of the out of plane displacement w, satisfying (4.1) and (4.2), near the tip of an extending crack in anti-plane shear and employs a technique first used in elastostatics by Knein [30] and Williams [31]. A similar approach was utilized by Freund and Clifton [32] in analyzing the near-tip displacement field for non-uniform crack propagation in plane strain. The procedure used here follows that of Achenbach and Bazant [33] who consider both the plane and anti-plane situations of non-uniform crack extension and obtain the lowest order near-tip displacement fields. The second order correction term in the displacement field near the crack tip is established here for non-uniform crack motion in anti-plane shear. In implementing the numerical simulation, we will use this more refined approximation during the initial stage of motion of the crack.

Consider the anti-plane problem of a straight crack extending non-uniformly in its plane along the x-axis say, with the crack tip position given by $x = \ell(s)$ at time t, where as before we let $s = ct$, c being the shear wave speed. Introducing the local polar coordinate system (R,θ), $-\pi \leq \theta \leq \pi$ at the moving crack tip (Fig. 5) through

$$x - \ell(s) = R\cos\theta \quad , \quad y = R\sin\theta \quad , \tag{7.1}$$

the displacement field $w = w(R,\theta,s)$ from (4.1) satisfies the differential equation;

$$w_{,RR} + \frac{1}{R} w_{,R} + \frac{1}{R^2} w_{,\theta\theta} = w_{,ss}$$

$$+ (\ell'(s)^2 \cos^2\theta) w_{,RR} - \left(\frac{\ell'(s)^2 \sin 2\theta}{R}\right) w_{,R\theta} + \left(\frac{\ell'(s)^2 \sin^2\theta}{R^2}\right) w_{,\theta\theta} \qquad (7.2)$$

$$+ \left(\frac{\ell'(s)^2 \sin^2\theta}{R}\right) w_{,R} + \left(\frac{\ell'(s)^2 \sin 2\theta}{R^2}\right) w_{,\theta} - 2(\ell'(s)\cos\theta)\, w_{,Rs} + 2\left(\frac{\ell'(s)\sin\theta}{R}\right) w_{,\theta s}$$

$$- (\ell''(s)\cos\theta) w_{,R} + \left(\frac{\ell''(s)\sin\theta}{R}\right) w_{,\theta} \quad .$$

It is now assumed that

$$w \sim R^m f(\theta,s) \quad \text{as} \quad R \to 0, \quad -\pi \le \theta \le \pi, \quad s \ge 0 \qquad (7.3)$$

for some non-negative exponent m. We seek the smallest value of $m \ge 0$ for which the above assumption is asymptotically consistent with the differential equation (7.2) and the traction-free boundary condition (4.2) on the crack surface. Calculating the derivatives of $w(R,\theta,s)$ given in (7.3) asymptotically as $R \to 0$, inserting the results into (7.2) and setting the dominant term in R equal to zero, one finds the following ordinary differential equation for $f(\theta,s)$:

$$\overline{P}(\theta) f_{,\theta\theta} - (m-1)\overline{P}_{,\theta}(\theta) f_{,\theta} + \{m(m-1)\left(\frac{1+\beta^2}{\beta^2}\right) + m(2-m)\overline{P}(\theta)\} f = 0 \quad , \qquad (7.4)$$

where $\overline{P}(\theta)$ and β are given by

$$\overline{P}(\theta) = 1 + \left(\frac{1-\beta^2}{\beta^2}\right)\cos^2\theta, \qquad \beta = \beta(s) = (1 - \ell'(s)^2)^{\frac{1}{2}} \quad . \qquad (7.5)$$

To solve (7.4), a new variable Θ is introduced through

$$\tan \Theta = \beta \tan \theta \quad . \tag{7.6}$$

For β given in (7.5) and $0 \leq \ell'(s) < 1$, Θ varies continuously from $-\pi$ to π as θ varies from $-\pi$ to π. In terms of Θ, $\overline{P}(\theta)$ now becomes

$$P(\Theta) = \overline{P}(\theta(\Theta)) = (1 - (1-\beta^2)\cos^2\Theta)^{-1} \quad . \tag{7.7}$$

Making the substitution

$$f(\theta,s) = P(\Theta)^{\frac{m}{2}} V(\Theta,s) \tag{7.8}$$

in (7.4) gives the following differential equation for v;

$$V_{,\Theta\Theta} + m^2 V = 0 \quad . \tag{7.9}$$

The traction-free boundary condition on the crack surface gives

$$f_{,\theta}(\pm\pi,s) = 0 \quad \text{which implies} \quad V_{,\Theta}(\pm\pi,s) = 0 \quad . \tag{7.10}$$

For displacement fields anti-symmetric about $y = 0$, as will be considered here, one has $w = 0$ on $y = 0$ giving $V(0,s) = 0$. The appropriate V satisfying (7.9) is then

$$V(\Theta,s) = A(s)\sin m\Theta \quad , \tag{7.11}$$

$A(s)$ being an arbitrary function of s and $\ell(s)$. The smallest value of m in (7.11) satisfying (7.10) is $m = \frac{1}{2}$. Combining (7.3),(7.8) and (7.11) now gives (see also [33]),

$$w \sim A(s)R^{\frac{1}{2}}P(\Theta)^{\frac{1}{4}}\sin\tfrac{1}{2}\Theta \quad \text{as} \quad R\to 0. \tag{7.12}$$

To find the second order correction term, let

$$w \sim R^{\frac{1}{2}}f(\theta,s) + R^{n}g(\theta,s) \quad \text{as} \quad R\to 0, \quad n>\tfrac{1}{2}\ , \tag{7.13}$$

where $f(\theta,s)$ is given by (7.8), (7.11) and $g(\theta,s)$ and n are to be determined. Again obtaining the derivatives of w asymptotically as $R\to 0$ from (7.13), putting them into (7.2) and considering the dominant term only, it can be shown that no non-trival function $g(\theta,s)$ exists for $1/2<n<3/2$. For $n = 3/2$, setting the dominant term in R to zero gives

$$\begin{aligned}\overline{P}(\theta)g_{,\theta\theta} - \tfrac{1}{2}\overline{P}_{,\theta}(\theta)g_{,\theta} + \{\tfrac{3}{4}\left(\frac{1+\beta^2}{\beta^2}\right) + \tfrac{3}{4}\,\overline{P}(\theta)\}g = \\ -\frac{1}{\beta^2}\{2A'(s)\ell'(s) + A(s)\ell''(s)\}\{\tfrac{1}{2}(\cos\theta)f - (\sin\theta)f_{,\theta}\} \\ -\frac{2}{\beta^2}A(s)\ell'(s)\{\tfrac{1}{2}(\cos\theta)f - (\sin\theta)f_{,\theta}\}_{,s}\ .\end{aligned} \tag{7.14}$$

Introducing Θ and $P(\Theta)$ as given by (7.6) and (7.7) respectively and making the substitution

$$g(\theta,s) = P(\Theta)^{\frac{3}{4}}Z(\Theta,s)\ , \tag{7.15}$$

equation (7.14) reduces to

$$\begin{aligned}Z_{,\Theta\Theta} + \frac{9}{4}Z = \frac{1}{2\beta}\,[2A'(s)\ell'(s) + \left(\frac{3-\beta^2}{2\beta^2}\right)A(s)\ell''(s)]\sin\tfrac{1}{2}\Theta \\ -\frac{(1-\beta^2)}{4\beta^3}A(s)\ell''(s)\sin\tfrac{5}{2}\Theta\ .\end{aligned} \tag{7.16}$$

The boundary conditions are $Z_{,\Theta}(\pm\pi, s) = 0$ and $Z(0,s) = 0$ as before. Solving (7.16) now for $Z(\Theta,s)$ and using (7.13), (7.15) gives the following expression for w in terms of Θ and s as $R \to 0$;

$$w \sim A(s)R^{\frac{1}{2}}P(\Theta)^{\frac{1}{4}}\sin\frac{1}{2}\Theta$$

$$+ R^{\frac{3}{2}}P(\Theta)^{\frac{3}{4}}\left[\left(\frac{A'(s)\ell'(s)}{2\beta} + \left(\frac{3-\beta^2}{8\beta^3}\right)A(s)\ell''(s)\right)\sin\frac{1}{2}\Theta + B(s)\sin\frac{3}{2}\Theta\right.$$

$$\left. + \frac{(1-\beta^2)}{16\beta^3}A(s)\ell''(s)\sin\frac{5}{2}\Theta\right] . \qquad (7.17)$$

Here $A(s)$, $B(s)$ are as yet arbitrary functions of s, and $\ell(s)$ also remains unspecified. The determination of $A(s)$ and $B(s)$ depends upon the region involved and the particular loading on the body. The error in (7.17) is $O(R^{5/2})$ as $R \to 0$.

Using the first term in (7.17) and the definition of the dynamic anti-plane shear stress intensity factor $K_d = K_d(s)$ given in (2.6), it can be established that

$$K_d(s) = \mu(\tfrac{\pi}{2})^{\frac{1}{2}}\beta^{\frac{1}{2}}A(s) . \qquad (7.18)$$

Then the expression for the energy release rate given in (2.7) becomes

$$G(s) = \frac{\pi\mu}{4}A(s)^2 . \qquad (7.19)$$

By virtue of the failure criterion (5.1) and (7.19), $A(s)$ is determined explicitly and is given by

$$A(s) = \left(\frac{4\Gamma}{\pi\mu}\right)^{\frac{1}{2}} \quad \text{for all } s, \tag{7.20}$$

where Γ is the specific fracture energy, assumed constant. $A(s)$ is then constant for all s, being independent of $\ell(s)$ also.

For the anti-plane shear edge crack problem discussed in Sections 3 and 4, $A(s)$ becomes

$$A \equiv A(s) = \frac{2\sqrt{2}}{\pi Q^{\frac{1}{2}}} \frac{w_o}{\ell_o^{\frac{1}{2}}} \quad \text{for all } s, \tag{7.21}$$

where Q is the dimensionless parameter given by (5.3), ℓ_o is the initial crack length and w_o is the fixed end displacement at $x = 0$ for $y > 0$ (Fig. 1(a)).

In a purely static problem, for a straight crack along the x axis with local polar coordinates r and α, $-\pi \le \alpha \le \pi$ situated at the fixed crack tip, the local displacement field at the crack tip under conditions of anti-plane shear is

$$w = D_1 r^{1/2} \sin\tfrac{1}{2}\alpha + D_2 r^{3/2} \sin\tfrac{3}{2}\alpha + O(r^{5/2}) \quad \text{as} \quad r \to 0 \quad . \tag{7.22}$$

This result may be established easily by employing the approach used in the moving crack tip case. Considering the initial static displacement field (3.3) for the edge crack problem in Section 3, it can easily be shown that

$$D_1 = \frac{2\sqrt{2}\, w_o}{\pi \ell_o^{1/2}} \quad \text{and} \quad D_2 = -\frac{w_o}{3\sqrt{2}\pi \ell_o^{3/2}} \quad . \tag{7.23}$$

Across the cylindrical wavefront $r = s$ generated by the initial motion of the crack tip, where r is the radial distance from the initial position of the crack tip at $x = \ell_o$, the following two conditions must hold;

(i) w is continuous across $r = s$ (7.24)

(ii) $\frac{\partial w}{\partial n} + \frac{\partial w}{\partial s}$ is continuous across $r = s$, (7.25)

where $\underline{n}$ is the unit outward normal to $r = s$. Since the material must maintain its physical integrity at the wavefront, equation (7.24) is necessary. Equation (7.25) guarantees that the impulse-momentum relation at the wavefront is satisfied. If (7.24) holds across $r = s$, it can easily be verified that (7.25) is also valid.

Equation (7.24) for $s \ll 1$ can be used to find $\ell'(0)$, $\ell''(0)$ and $B(0)$. Equating (7.17), (7.21) with (7.22), (7.23) on $r = s$ correct to $O(s^{\frac{1}{2}})$ for $s \ll 1$ gives

$$\ell'(0) = \frac{Q^2-1}{Q^2+1} \quad . \tag{7.26}$$

This is in agreement with equation (5.6) which results from the exact differential equation governing the motion of the tip. Matching correct to $O(s^{3/2})$ on $r = s$ for $s \ll 1$ gives

$$\ell''(0) = -\ell'(0)(1 - \ell'(0)^2)/4\ell_o \tag{7.27}$$

and

$$B(0) = A[16 + 5\ell'(0) + 3\ell'(0)(1 - \ell'(0)^2)] / 192\,\ell_o\,(1 - \ell'(0)^2) \quad , \tag{7.28}$$

where A is given in (7.21). Equation (7.17) used in conjunction with (7.21), (7.26), (7.27) and (7.28) now gives the dynamic displacement field near the moving crack tip for $s \ll 1$.

8. Finite difference formulation of the edge crack problem

Here we consider the numerical solution of the dynamic anti-plane shear edge crack problem formulated and discussed in Sections 2,3 and 4. The two-dimensional wave equation (4.1) governing the motion of a body in a state of infinitesimal anti-plane shear must be satisfied in the half-plane $x \geq 0$, excluding the crack. The body is assumed to be initially at rest and the boundary conditions are given by (4.2) and (4.3). The initial static solution for the edge crack problem is given in (3.3). The problem as formulated is anti-symmetric about $y = 0$ and hence we need only consider the region $x \geq 0$, $y \geq 0$.

A. Finite difference equations

To approximate the equation of motion (4.1) by a finite difference equation in the region $x \geq 0$, $y \geq 0$, we introduce a rectangular grid of mesh size $\Delta x = \Delta y = h$ in the x and y directions together with a time increment Δs. The grid nodes are located at (see Fig. 6)

$$x = (i-1)h, \quad y = (j-\tfrac{1}{2})h; \quad i,j = 1,2,3,\text{----} \quad . \tag{8.1}$$

The displacement w at the time step $s = k\Delta s$ and at a mesh point (x,y) given in (8.1) is denoted by

$$w^k_{i,j} = w(x,y,s) \quad ; \quad \begin{matrix} i,j = 1,2,3,\text{----} \\ k = 0,1,2,\text{----} \end{matrix} \quad . \tag{8.2}$$[1]

Let P denote the triad $((i-1)h, (j-\frac{1}{2})h, k\Delta s)$. Using central differences, we have

[1] Note that in $w^k_{i,j}$ the comma preceding the subscript j does not denote partial differentiation.

$$w_{,ss}(P) = \left(w_{i,j}^{k+1} - 2w_{i,j}^{k} + w_{i,j}^{k-1}\right) \Big/ \Delta s^2 + O(\Delta s^2) \quad . \tag{8.3}$$

For $w_{,xx}(P) + w_{,yy}(P)$, we use the nine node approximation:

$$w_{,xx}(P) + w_{,yy}(P) = [(w_{i-1,j-1}^{k} + w_{i-1,j+1}^{k} + w_{i+1,j-1}^{k} + w_{i+1,j+1}^{k})$$

$$+ 4(w_{i-1,j}^{k} + w_{i,j-1}^{k} + w_{i,j+1}^{k} + w_{i+1,j}^{k}) - 20w_{i,j}^{k}] \Big/ 6h^2 + O(h^2) \tag{8.4}$$

Equation (8.4) was found to be more satisfactory than that which makes use of the usual central difference approximations for $w_{,xx}(P) + w_{,yy}(P)$. Accordingly from (8.3) and (8.4), we get the following finite difference approximation for the wave equation (4.1);

$$w_{i,j}^{k+1} = 2w_{i,j}^{k} - w_{i,j}^{k-1} + \frac{\rho^2}{6} [(w_{i-1,j-1}^{K} + w_{i-1,j+1}^{k} + w_{i+1,j-1}^{k} + w_{i+1,j+1}^{k})$$

$$+ 4(w_{i-1,j}^{k} + w_{i,j-1}^{k} + w_{i,j+1}^{k} + w_{i+1,j}^{k}) - 20w_{i,j}^{k}] \quad , \tag{8.5}$$

where $\rho = \Delta s/h$. Equation (8.5) is a three-level explicit difference scheme, accurate to $O(h^2 + \Delta s^2)$, and hence it is possible to compute the displacement at time step $s = (k+1)\Delta s$ whenever its values at the two previous time steps $s = (k-1)\Delta s$ and $s = k\,\Delta s$ are known everywhere.

The boundary condition (4.3), that is $w = w_o$ on $x = 0$, $y \geq 0$, gives

$$w_{1,j}^{k} = w_o \quad , \qquad \begin{matrix} j = 1,2,3,\text{----} \\ k = 0,1,2,\text{----} \end{matrix} \quad . \tag{8.6}$$

To accommodate the boundary conditions on $y = 0$, a line of auxillary grid points located at $y = -h/2$ outside the medium is introduced (Fig. 6). The crack plane is on $y = 0$ and the crack length at time s is $\ell(s)$ as before. For $0 \le x < \ell(s)$ the free surface boundary condition yields $w_{,y}(x,0,s) = 0$, which on approximating by central differences across $y = 0$ gives

$$w^k_{i,-1} = w^k_{i,1} \quad , \tag{8.7}$$

for all i such that $0 \le (i-1)h < \ell(k\,\Delta s)$. For $x \ge \ell(s)$, anti-symmetry with respect to $y = 0$ gives $w(x,0,s) = 0$ and also $w(x,-h/2,s) = -w(x,h/2,s)$, which yields

$$w^k_{i,-1} = -w^k_{i,1} \quad , \tag{8.8}$$

for all i such that $(i-1)h > \ell(k\,\Delta s)$.

Placing the grid points on $y = -h/2,\ h/2,\ 3h/2,$---- was found superior to putting them on $y = 0,\ h,\ 2h,$----, thereby having grid nodes on the crack plane and in the path of the crack tip. Equations (8.7) and (8.8) approximate the boundary conditions on $y = 0$ for $x < \ell(s)$ and $x \ge \ell(s)$ respectively, correct to $O(h^2)$ away from the crack tip. Because of the singular displacement gradients at the tip itself, the finite difference equation (8.5) and the corresponding boundary conditions (8.7) and (8.8) cannot be expected to be very accurate close to the tip. Additional measures are necessary to accurately approximate the displacement field near the moving crack tip.

B. Stability Analysis

To apply the proposed finite difference formula (8.5), stability criteria must be established which guarantee that the difference between the numerical and theoretical solution of the difference equation (8.5) does not grow with time. The analysis performed here follows von Neumann's method [34]. As will be shown in the following, the stability requirement will impose restrictions on the possible values of the time increment Δs in relation to the mesh size h and possibly other variables in the problem.

The stability of (8.5) may be examined by assuming that an error $z^k_{i,j}$ exists at each mesh point ($k = 0, 1, 2, \text{----}$). Since the difference equation (8.5) is linear and has constant coefficients, the growth of these errors is governed by (8.5) with $w^k_{i,j}$ replaced by $z^k_{i,j}$. Performing a harmonic decomposition of the errors at a given time level, say $s = 0$, gives

$$z^0_{i,j} = \sum_{i,j} A_{ij} e^{(-1)^{\frac{1}{2}}\beta_{ij} ih} e^{(-1)^{\frac{1}{2}}\gamma_{ij} jh} , \qquad (8.9)$$

where the frequencies β_{ij} and γ_{ij} are arbitrary in general and the summation over i and j ranges over all the grid points (finite in number) in the x and y directions, respectively. Since the difference equation is linear, to examine the growth of these errors, it is necessary to consider only the single term

$$z^0_{i,j} = e^{(-1)^{\frac{1}{2}}\beta ih} e^{(-1)^{\frac{1}{2}}\gamma jh} , \qquad (8.10)$$

where β and γ can be any real numbers.

To investigate the error propagation, we now seek a solution to (8.5) with $w^k_{i,j}$ replaced by $z^k_{i,j}$ which reduces to (8.10) at $s = 0$. A solution of the difference system (8.5), obtained by separating the variables with (8.10) in mind, is

$$z^k_{i,j} = R_k e^{(-1)^{\frac{1}{2}}\beta ih}\, e^{(-1)^{\frac{1}{2}}\gamma jh} , \tag{8.11}$$

where R_k satisfies

$$R_{k+1} - 2BR_k + R_{k-1} = 0 , \quad B = 1 - \rho^2 A/2 , \tag{8.12}$$

and

$$A = 4[\sin^2(\tfrac{\beta h}{2}) - \tfrac{2}{3}\sin^2(\tfrac{\beta h}{2})\sin^2(\tfrac{\gamma h}{2}) + \sin^2(\tfrac{\gamma h}{2})] . \tag{8.13}$$

The general solution to (8.12) is found on letting $R_k = \eta^k$ which gives

$$\eta^2 - 2B\eta + 1 = 0 , \tag{8.14}$$

or $\eta = B \pm \sqrt{B^2-1}$. The errors $z^k_{i,j}$ will not grow provided $|\eta| < 1$, which leads to

$$0 < \rho^2 A < 4 . \tag{8.15}$$

From (8.13), it may be easily verified that $0 \le A \le 16/3$, which on using (8.15) gives $\rho < \sqrt{3}/2$. Hence round-off error will not grow and the difference scheme (8.5) will be stable provided

$$\rho = \frac{\Delta s}{h} < \frac{\sqrt{3}}{2} . \tag{8.16}$$

9. Numerical simulation procedure of crack motion and results

A. Simulation procedure and crack tip velocity determination

At each time step during the numerical process, the velocity of the crack tip must be determined. The crack tip velocity is needed in calculating the position of the crack tip at the next time step and also is required in utilizing the asymptotic displacement field in the vicinity of the moving crack tip. A procedure for determining the crack tip velocity is now presented.

Consider a region D_s in the (x,y) - plane containing the crack tip in its interior and hence having a portion of the crack surface as part of its boundary (Fig. 5). The region D_s is assumed to move with the velocity of the tip parallel to the x-axis. The energy contained within D_s at time s is given by

$$E_{D_s} = \int_{D_s} (W + K)dxdy \quad , \tag{9.1}$$

where W and K represent the potential and kinetic energies respectively of the body per unit volume. For any closed contour C_s surrounding the crack tip and moving with the velocity of the tip parallel to the x-axis, the rate at which energy is entering through C_s is given by the contour integral

$$E_{C_s} = c \oint_{C_s} [\mu \frac{\partial w}{\partial n} \frac{\partial w}{\partial s} + \ell'(s)(W + K)n_x]dC_s \quad , \tag{9.2}$$

where $\underline{n} = (n_x, n_y)$ is the unit outward normal to C_s and c is the shear wave speed. Letting C_s be the boundary of D_s excluding the crack surface, then the flux of energy through C_s given in (9.2) must equal

the rate of change of kinetic and potential energy within D_s plus the rate at which energy is being dissipated by the moving crack tip. Note that there is no contribution to E_{C_s} in (9.2) from a traction-free crack surface along the x-axis. Hence we have the following relation (see [10] also);

$$G\ell'(s) = \oint_{C_s} [\mu \frac{\partial w}{\partial n} \frac{\partial w}{\partial s} + \ell'(s)(W+K)n_x]dC_s - \frac{d}{ds} \int_{D_s} (W+K)dxdy \ , \qquad (9.3)$$

where G is the energy release rate. Equation (9.3) may be rewritten as

$$\left(G - \oint_{C_s} (W+K)n_x dC_s\right) \ell'(s) = \mu \oint_{C_s} (\frac{\partial w}{\partial n} \frac{\partial w}{\partial s})\, dC_s - \frac{d}{ds} \int_{D_s} (W+K)dxdy \ , \qquad (9.4)$$

giving an equation for the crack tip velocity $\ell'(s)$.

For a linear elastic body in anti-plane shear,

$$W = \frac{\mu}{2} (w,_x^2 + w,_y^2) \quad \text{and} \quad K = c^2 \frac{\rho}{2} w,_s^2 \ . \qquad (9.5)$$

The energy release rate G in (9.4) is given by (7.19) and (7.21). Then knowing the gradients of the displacement in a region about the moving crack tip, equation (9.4) enables us to calculate the velocity of the tip. This must be done using the numerical displacement field.

As was noted in Section 8, the finite difference equation (8.5) cannot be expected to be very accurate at the mesh points closest to the moving crack tip. To alleviate this difficulty the lowest order asymptotic displacement term (7.12), with A(s) given by (7.21), is used at the two nodal points in the region nearest to the crack tip i.e. at (LN,1) and (LN+1,1), where $i = LN$ and $j = 1$ denote the mesh point nearest to the

tip and to the left of it. To smooth the transition from the asymptotic to the numerical values of the displacement as the tip moves, a linear combination of both the asymptotic and numerical displacement values is used at the four nodal points (LN-1,1), (LN,2), (LN+1,2) and (LN+2,1) surrounding the tip. The linear combination used is $[\alpha w^{k}_{i,j}+(h-\alpha)w_{as}]/h$, where w_{as} denotes the lowest order near-tip asymptotic displacement given in (7.12) and $\alpha = [\ell(k\Delta s)-(LN-1)h]$ is the distance of the tip from $i = LN$.

Before calculating the crack tip velocity for the present or k^{th} time step, the lowest order asymptotic near-tip displacement (7.12) is used as outlined in the preceding paragraph together with the crack tip velocity of the previous or $(k-1)^{st}$ time step. After determining the velocity of the tip for the k^{th} time step, equation (7.12) is then used again with this new crack tip velocity to provide the near-tip asymptotic displacement for the current time step. Knowing the crack tip position $\ell(k\Delta s)$ and velocity $\ell'(k\Delta s)$ at the k^{th} time step, the position of the tip at the next time step is given by

$$\ell((k+1)\Delta s) = \ell(k\Delta s) + \ell'(k\Delta s)\Delta s \quad , \tag{9.6}$$

correct to $O(\Delta s^2)$.

To initiate the motion of the crack tip, the near-tip asymptotic displacement including the second-order correction term given by equation (7.17) is used in conjunction with (7.21), (7.27) and (7.28) at the appropriate mesh points near the tip for the first four time steps. The crack tip position and velocity used with equation (7.17) for these first four time steps is given by

$$\ell(s) = \ell(0) + \ell'(0)s + \frac{1}{2}\ell''(0)s^2 \tag{9.7}$$

and

$$\ell'(s) = \ell'(0) + \ell''(0)s \quad , \tag{9.8}$$

where $\ell'(0)$ and $\ell''(0)$ are given in (7.26) and (7.27) respectively. To facilitate further the initiation of the numerical process, equations (9.7) and (9.8) are used to give the crack tip position and velocity for the first ten time steps. This is justified for sufficiently small time increments Δs since the error in (9.7) and (9.8) is $O(s^3)$ and $O(s^2)$ respectively for $s \ll 1$. Thereafter the crack tip velocity is found numerically.

To determine the crack tip velocity from equation (9.4), the time rate of change of the kinetic and potential energy in the region D_s, i.e. the last term in (9.4), must be evaluated numerically. However, because of transient disturbances introduced into the numerical values of the displacement by the motion of the crack tip, the accurate calculation of the last term in (9.4) proved to be very difficult. Using the lowest order asymptotic expression for the displacement near the crack tip (7.12), it can be shown that

$$\frac{d}{ds}\int_{D_s}(W+K)dxdy = O(h) \quad \text{as} \quad h \to 0 \quad . \tag{9.9}$$

Then taking a very small contour C_s about the crack tip and neglecting the last term in (9.4) gives the following equation which approximates $\ell'(s)$ correct to $O(h)$ as $h \to 0$,

$$\left(G - \oint_{C_s} (W + K) n_x dC_s \right) \ell'(s) = \mu \oint_{C_s} \left(\frac{\partial w}{\partial n} \frac{\partial w}{\partial s} \right) dC_s \quad . \tag{9.10}$$

From equation (9.6) the crack tip position for the next time can then be estimated correct to $O(h^2)$. The energy release rate G is given by (7.19), (7.21) and substituting for W and K from (9.5), equation (9.10) becomes

$$\left(\frac{2w_o^2}{\pi Q \ell_o} - \oint_{C_s} \frac{1}{2} \left[\left(\frac{\partial w}{\partial x} \right)^2 + \left(\frac{\partial w}{\partial y} \right)^2 + \left(\frac{\partial w}{\partial s} \right)^2 \right] n_x dC_s \right) \ell'(s) = \oint_{C_s} \left(\frac{\partial w}{\partial n} \frac{\partial w}{\partial s} \right) dC_s \tag{9.11}$$

with Q given in (5.3).

In Fig. 6, the upper-half of the contour C_s used in finding the velocity of the crack tip is illustrated. The contour is fixed relative to the tip for all time since it moves with the velocity of the tip. From the symmetry inherent in the problem, it is sufficient to evaluate the integrals in the upper half-plane. The vertical segments of the contour are a distance $2h$ ahead and behind the crack tip, while the horizontal portion is along $j = 3$. To evaluate the contour integrals in (9.11), the displacement gradients $w_{,x}$, $w_{,y}$ and $w_{,s}$ must be found at points along the contour. At the mesh points adjacent to or on the contour, the spatial gradients $w_{,x}$ and $w_{,y}$ are found using the central difference approximation. To find $w_{,s}$ at the grid node (i,j) and at the time step $s = k \Delta s$, the following difference approximation is used

$$\left(\frac{\partial w}{\partial s} \right)_{i,j}^{k} = \left(3w_{i,j}^{k} - 4w_{i,j}^{k-1} + w_{i,j}^{k-2} \right) / (2 \Delta s) \quad . \tag{9.12}$$

The error in (9.12) is $O(\Delta s^2)$ and for the $(k-2)^{nd}$ time step it is only necessary to keep the values of the displacement at the required mesh points near the tip. The integrals along the top segment of the contour are evaluated using the three point Simpson's rule, while the integrals along the vertical segments are evaluated using a three-point formula with integration points at $y = h/2$, $3h/2$ and $5h/2$, which is exact for cubic polynomials. At a requisite point on the contour, the displacement gradients are found using a linear combination of the values of the corresponding gradients at the two nearby grid nodes, one to the right and one to the left of the point under consideration. This gives the displacement gradients at the integration points on the contour correct to $O(h^2)$. The normalized crack tip velocity $\ell'(s)$ can now be found from equation (9.11).

B. Stress intensity factor determination

To find the dynamic stress intensity factor K_d at the moving crack tip, we note that from equations (7.18) and (7.5) that

$$K_d(s) = (\tfrac{\pi}{2})^{\frac{1}{2}} \mu (1 - \ell'(s)^2)^{\frac{1}{4}} A(s) \quad , \tag{9.13}$$

where $A(s)$ is the time-dependent function in the expression for the lowest order asymptotic displacement near the tip in (7.12). Normalizing $K_d(s)$ with respect to the initial static stress intensity factor K_{st} given in (3.8), equation (9.13) becomes

$$\frac{K_d(s)}{K_{st}} = \frac{\pi \ell_0^{\frac{1}{2}}}{2\sqrt{2}\, w_0} (1 - \ell'(s)^2)^{\frac{1}{4}} A(s) \quad . \tag{9.14}$$

As the crack is propagating, the failure criterion (5.1) applies; it yields the previously derived expression in equation (7.21) for $A(s)$. Using (7.21), equation (9.14) reduces to

$$\frac{K_d(s)}{K_{st}} = (1 - \ell'(s)^2)^{\frac{1}{4}} / Q^{\frac{1}{2}} \quad , \tag{9.15}$$

and this equation is valid while the crack is extending i.e. $\ell'(s)>0$. Hence up to the time of arrest, the stress intensity factor may be easily calculated, once the crack tip velocity is determined from the numerical solution.

After arrest the failure criterion is no longer valid, and the stress intensity factor must be evaluated directly from the numerical solution. Equation (7.12) is still valid after arrest with $\ell'(s)$ equal to zero. Consider now the upper-half of the contour C_s, used in evaluating the crack tip velocity $\ell'(s)$ in (9.11), which we denote by C_*. The position of C_* is now fixed after arrest relative to the stationary tip. To evaluate the stress intensity factor, we consider the contour integral

$$I = \int_{C_*} w \, dC_* \quad . \tag{9.16}$$

Using for w the lowest order asymptotic displacement term near the tip given in (7.12) and evaluating the contour integral analytically gives

$$I = \int_{C_*} w \, dC_* = \frac{4\sqrt{2}}{3} [1 - (5+(41)^{\frac{1}{2}})^{\frac{1}{2}} - 5(5+(41)^{\frac{1}{2}})^{-\frac{1}{2}}] A(s) h^{\frac{3}{2}} + O(h^{\frac{5}{2}}) \quad . \tag{9.17}$$

Rewriting equation (9.17) gives the following approximation to $A(s)$;

$$A(s) = \frac{3}{4\sqrt{2}} h^{-\frac{3}{2}} [1 - (5+(41)^{\frac{1}{2}})^{\frac{1}{2}} - 5(5+(41)^{\frac{1}{2}})^{-\frac{1}{2}}]^{-1} \int_{C_*} w \, dC_* \, . \qquad (9.18)$$

The contour integral in (9.18) is calculated in a similar manner to the way in which the contour integrals in (9.11) were evaluated when determining the crack tip velocity. This enables us to determine $A(s)$. Equation (9.14) with $\ell'(s)$ set equal to zero and equation (9.18) then give the stress intensity factor after arrest.

C. Numerical results

In the numerical results presented here, the exact initial static displacement field (3.3) is used at all grid points in the mesh at $s = 0$. The time increment taken at each time step is $\Delta s = h/2$, which satisfies the stability requirement (8.16). Considering the dimensionless variables x/ℓ_0, y/ℓ_0, s/ℓ_0 and w/w_0 as done in Section 5 for the analytical case, then the problem depends only on the dimensionless parameter Q, defined in (5.3). As in the analytical case, $Q = 1.5$ is taken here.

Plots of the crack tip velocity and crack length evaluated numerically up to the time of arrest are shown in Figs. 7 and 8. The mesh size employed is $\Delta x = \Delta y = h = .02$, while the number of grid points used for the quarter-plane $x \geq 0$, $y \geq 0$ is (150,90). For the value of h under consideration this ensures that the outer boundary effects arising from the finite grid do not affect the results. In Fig. 7 the normalized crack tip velocity $\ell'(s) = \dot{\ell}(t)/c$, calculated numerically using (9.11), is plotted against $s = ct$ and compared with the exact tip velocity acquired in Section 5.

The numerically evaluated velocity tends to oscillate slightly as the crack tip traverses the grid, but overall the agreement with the exact solution is quite good. The reflected wavefront from the boundary at $x = 0$ is smoothed out in the numerical solution and hence the tip velocity as determined from the numerical solution does not exhibit the abrupt corner present in the exact solution when this wave reaches the crack tip. This is to be expected, since the difference sheme cannot propagate a sharp wavefront. In Fig. 8 the normalized crack length $\ell(s)/\ell_o$ is plotted against $s/\ell_o = ct/\ell_o$ up to arrest and shows excellent agreement with the exact solution.

The numerically calculated stress intensity factor $K_d(s)$, normalized by the initial static stress intensity factor K_{st}, is shown in Fig. 9 up to the time that the second reflected wave reaches the tip from the end $x = 0$. The mesh size used in Fig. 9 is $h = .04$ while the number of grid points is (150,90) as before. Before crack arrest $K_d(s)$ is determined using equation (9.15) together with the numerically evaluated crack tip velocity, while after arrest equations (9.14) and (9.18) are used. The reflected stress waves return to the tip slightly faster in the numerical than in the analytical solution because the wavefronts are being dispersed somewhat in the numerical scheme as time increases.

Overall the numerical results agree remarkably well with the exact solution. The accuracy of these results increases for smaller values of h. Also the smaller the value of Δs relative to h , the better the results, primarily because more time steps are then used in traversing the grid, and this leads to a smoother velocity profile. Care must be exercised in using the asymptotic solution near the moving tip to avoid introducing unwanted oscillations into the crack tip velocity. The method

presented herein for avoiding such oscillations as much as possible was found to be the most satisfactory.

10. Further applications

All of the work presented in this study has been for infinitesimal anti-plane shear deformations. In plane strain crack propagation problems, two non-zero displacement components are present, as well as both dilatation and shear waves. This, together with more complicated wave reflection patterns at the specimen boundaries makes plane strain problems, especially for finite regions, far more difficult. Therefore one must resort to a numerical approach. As in anti-plane shear, the stress and particle velocity fields are singular at the moving tip and hence must be adequately approximated in a numerical simulation.

The lowest order asymptotic displacement field near the tip of a propagating crack in plane strain is available for non-uniform crack velocity in [32] and so can be incorporated into a suitable finite difference scheme in order to accurately represent the elastodynamic field near a propagating crack tip. It should be possible to accomplish this without a lot of difficulty, not only for the case of known crack history, but where the crack history is to be determined using a suitable failure criterion as well.

It would be of interest to apply the finite difference technique incorporating the local displacement field near a crack tip to some plane strain crack propagation problems already studied and compare with such exact results as are available or with other numerical solutions. An interesting problem suitable for numerical study is the plane strain analogue of the edge crack problem analyzed herein. For a constant displacement in the positive y direction and an equal and opposite displacement in the negative y direction at the boundary $x = 0$, thus separating

the crack surfaces; then for fixed or traction-free conditions normal to the end $x = 0$, one could study the effect of the individual reflected stress waves from $x = 0$ on the motion of the tip and check if and when crack arrest might occur.

The anti-plane shear work discussed in this investigation has been carried out for infinitesimal deformations in linear elastic materials. Knowles [35] has studied the elastic field near the tip of a stationary crack for a class of fully nonlinear elastic materials subjected to finite deformations. It would be interesting to consider the dynamic problem of a rapidly extending crack in a nonlinear elastic material taking finite deformations into account. The local displacement field near a moving crack tip may be derived, as in Section 7, for different classes of nonlinear materials. This could then be used with a finite difference scheme to model the problem, and thus to study the effect of nonlinearity on the crack tip motion.

REFERENCES

[1] B.V. Kostrov, Unsteady propagation of longitudinal shear cracks, Journal of Applied Mathematics and Mechanics (English translation of PMM), 30 (1966) 1241.

[2] J.D. Eshelby, The elastic field of a crack extending non-uniformly under general anti-plane loading, Journal of the Mechanics of Physics and Solids, 17 (1969) 177.

[3] L.B. Freund, Crack propagation in an elastic solid subjected to general loading-II. Non-uniform rate of extension, Journal of the Mechanics of Physics and Solids, 20 (1972) 141.

[4] B.V. Kostrov, Crack propagation at variable velocity, International Journal of Fracture, 11 (1975) 47.

[5] T.C. Kennedy and J.D. Achenbach, Extension of a cut-induced crack under antiplane loading, Journal of Elasticity, 3 (1973) 277.

[6] J.D. Achenbach, Extension of a crack by a shear wave, ZAMP, 21 (1970) 887.

[7] J.D. Achenbach, Crack propagation generated by a horizontally polarized shear wave, Journal of the Mechanics of Physics and Solids, 18 (1970) 947.

[8] A.E. Molchanov and L.V. Nikitin, Dynamics of longitudinal shear cracks after the loss of stability, Mechanics of Solids (English translation of MTT), 7 (1972) 55.

[9] P.H. Melville, Effect of reflected stress waves on the stress intensity factor of an anti-plane strain edge crack during crack propagation and after crack arrest, International Journal of Fracture, 17 (1981) 3.

[10] C. Atkinson and J.D. Eshelby, The flow of energy into the tip of a moving crack, International Journal of Fracture, 4 (1968) 3.

[11] J.R. Rice, Mathematical analysis in the mechanics of fracture, Fracture, Vol. 2, edited by H. Liebowitz, Academic Press, New York, (1968) 191.

[12] J.D. Achenbach, Dynamic effects in brittle fracture, Mechanics Today, edited by S. Nemat-Nasser, Pergamon Press, New York, (1974) 1.

[13] J. Miklowitz, The Theory of Elastic Waves and Waveguides, North-Holland, New York, (1978) 363.

[14] M.F. Kanninen, A critical appraisal of solution techniques in dynamic fracture mechanics, Numerical Methods in Fracture Mechanics, edited by A.R. Luxmoore and D.R.J. Owen, University College of Swansea, Wales, (1978) 612.

[15] R.H. Gallagher, A review of finite element techniques in fracture mechanics, Numerical Methods in Fracture Mechanics, edited by A.R. Luxmoore and D.R.J. Owen, University College of Swansea, Wales, (1978) 1.

[16] J.A. Aberson, J.M. Anderson and W.W. King, Dynamic analysis of cracked structures using singularity finite elements, Elastodynamic Crack Problems, Mechanics of Fracture 4, edited by G.C. Sih, Noordoff International Publishing, Leyden, (1977) 249.

[17] J.A. Aberson, J.M. Anderson and W.W. King, Singularity-element simulation of crack propagation, Fast Fracture and Crack Arrest, ASTM STP 627, edited by G.T. Hahn and M.F. Kanninen, American Society for Testing and Materials, (1977) 123.

[18] W.W. King, J.F. Malluck, J.A. Aberson and J.M. Anderson, Application of running-crack eigenfunctions to finite-element simulation of crack propagation, Mechanics Research Communications, 3 (1976) 197.

[19] S. Aoki, K. Kishimoto, H. Kondo and M. Sakata, Elastodynamic analysis of crack by finite element method using singular element, International Journal of Fracture, 14 (1978) 59.

[20] K. Kishimoto, S. Aoki and M. Sakata, Computer simulation of fast crack propagation in brittle material, International Journal of Fracture, 16 (1980) 3.

[21] T. Nishioka and S.N. Atluri, Numerical modeling dynamic crack propagation in finite bodies, by moving singular elements — Part 1: Formulation, Part 2: Results, Journal of Applied Mechanics, 47 (1980) 570.

[22] T. Nishioka and S.N. Atluri, Numerical analysis of dynamic crack propagation: generation and prediction studies, Engineering Fracture Mechanics, 16 (1982) 303.

[23] M. Shmuely and D. Peretz, Static and dynamic analysis of the DCB problem in fracture mechanics, International Journal of Solids and Structures, 12 (1976) 67.

[24] T. Kanazawa and S. Machida, Energy considerations in dynamic crack propagation and arrest, Proceedings, Fourth International Conference on Fracture, edited by D.M.R. Taplin, Waterloo, Canada, (1977) 223.

[25] H. Stöckl and F. Auer, Dynamic behavior of a tensile crack: finite difference simulation of fracture experiments, International Journal of Fracture, 12 (1976) 345.

[26] J. Aboudi, Numerical solution of dynamic stresses induced by moving cracks, Computer Methods in Applied Mechanics and Engineering, 9 (1976) 301.

[27] M. Shmuely and M. Perl, The SMF2D code for proper simulation of crack propagation, Crack Arrest Methodology and Applications, ASTM STP 711, edited by G.T. Hahn and M.F. Kanninen, American Society for Testing and Materials, (1980) 54.

[28] M. Perl, M. Shmuely and D. Peretz, An improved dynamic crack propagation simulation in the SEN specimen by the SMF2D code, International Journal of Fracture, 19 (1982) 17.

[29] P. Burgers, Dynamic linear elastic crack propagation in anti-plane shear by finite differences, International Journal of Fracture, 16 (1980) 261.

[30] M. Knein, Zur theorie des druckversuchs, Abhandlungen aus dem aerodynamischen Institut an der T.H. Aachen, 7 (1927) 62.

[31] M.L. Williams, Stress singularities resulting from various boundary conditions in angular corners in extension, Journal of Applied Mechanics, 19 (1952) 526.

[32] L.B. Freund and R.J. Clifton, On the uniqueness of plane elastodynamic solutions for running cracks, Journal of Elasticity, 4 (1974) 293.

[33] J.D. Achenbach and Z.P. Bazant, Elastodynamic near-tip stress and displacement fields for rapidly propagating cracks in orthotropic materials, Journal of Applied Mechanics, 42 (1975) 183.

[34] A.R. Mitchell and D.V. Griffiths, The Finite Difference Method in Partial Differential Equations, Wiley, (1980) 38.

[35] J.K. Knowles, The finite anti-plane shear field near the tip of a crack for a class of incompressible elastic solids, International Journal of Fracture, 13 (1977) 611.

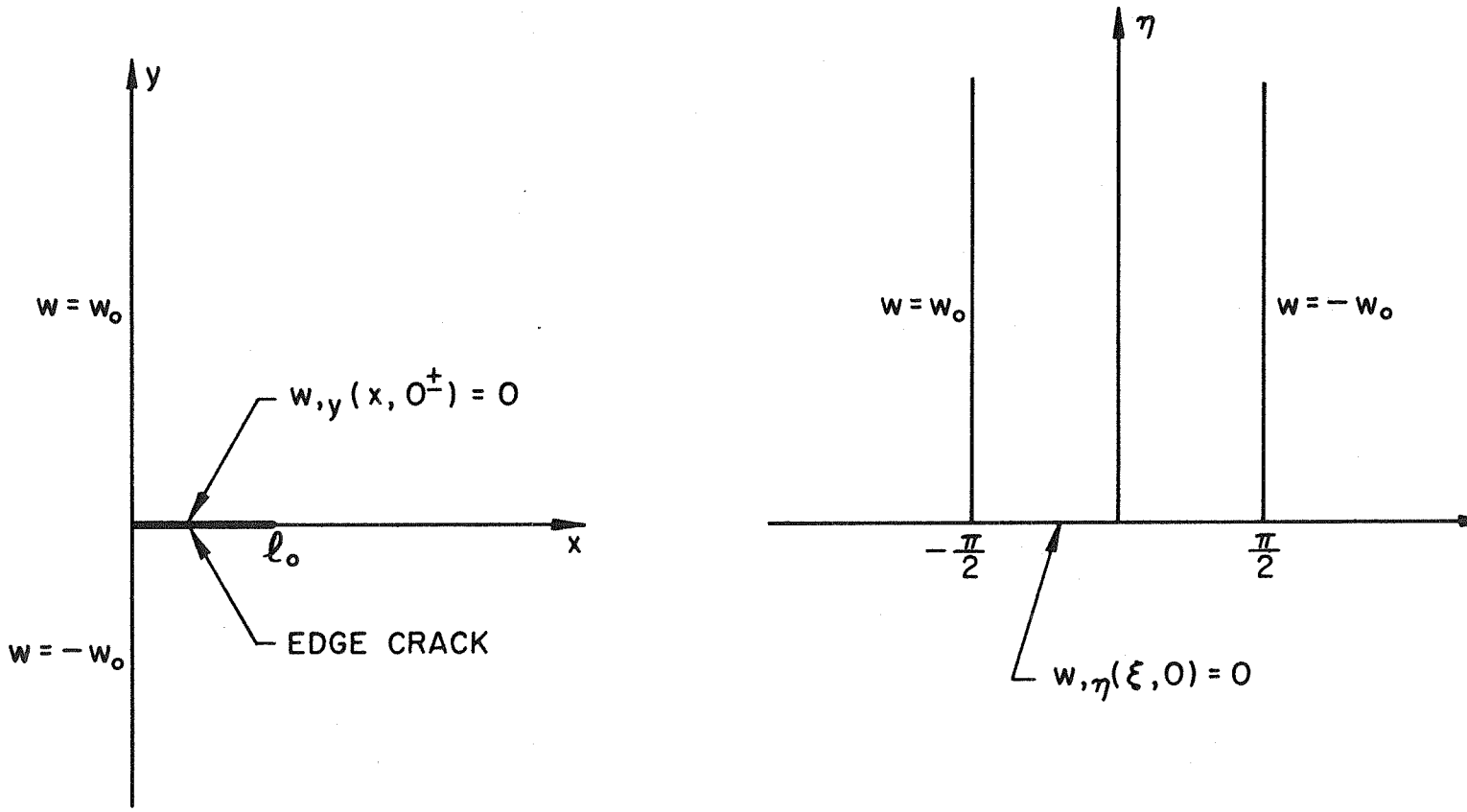

Figure 1. Initial static configuration and its image under mapping (3.2) in the $\xi - \eta$ plane.

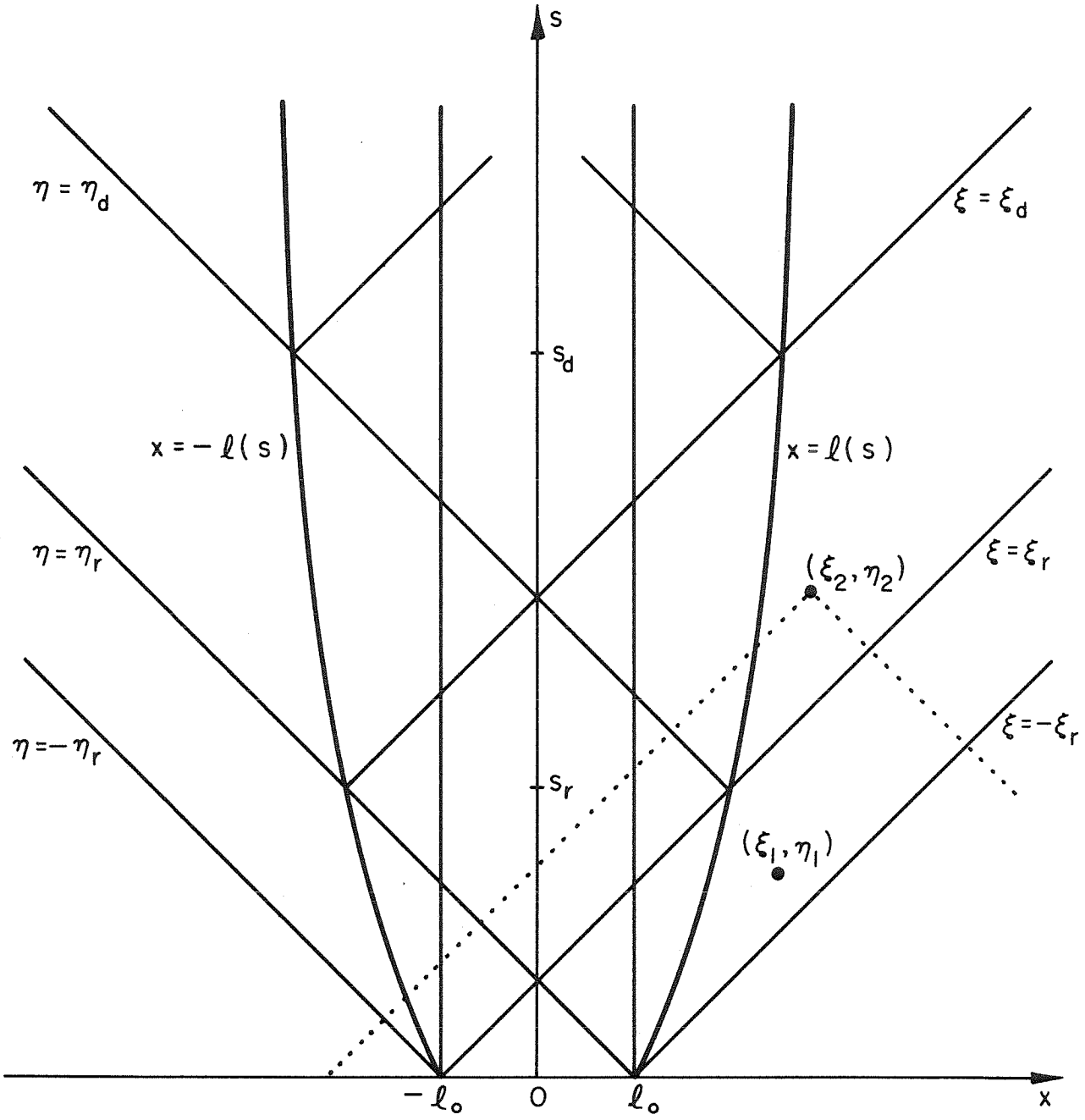

Figure 2. The x - s plane showing crack tip trajectories $x = \pm\ell(s)$ and wavefronts.

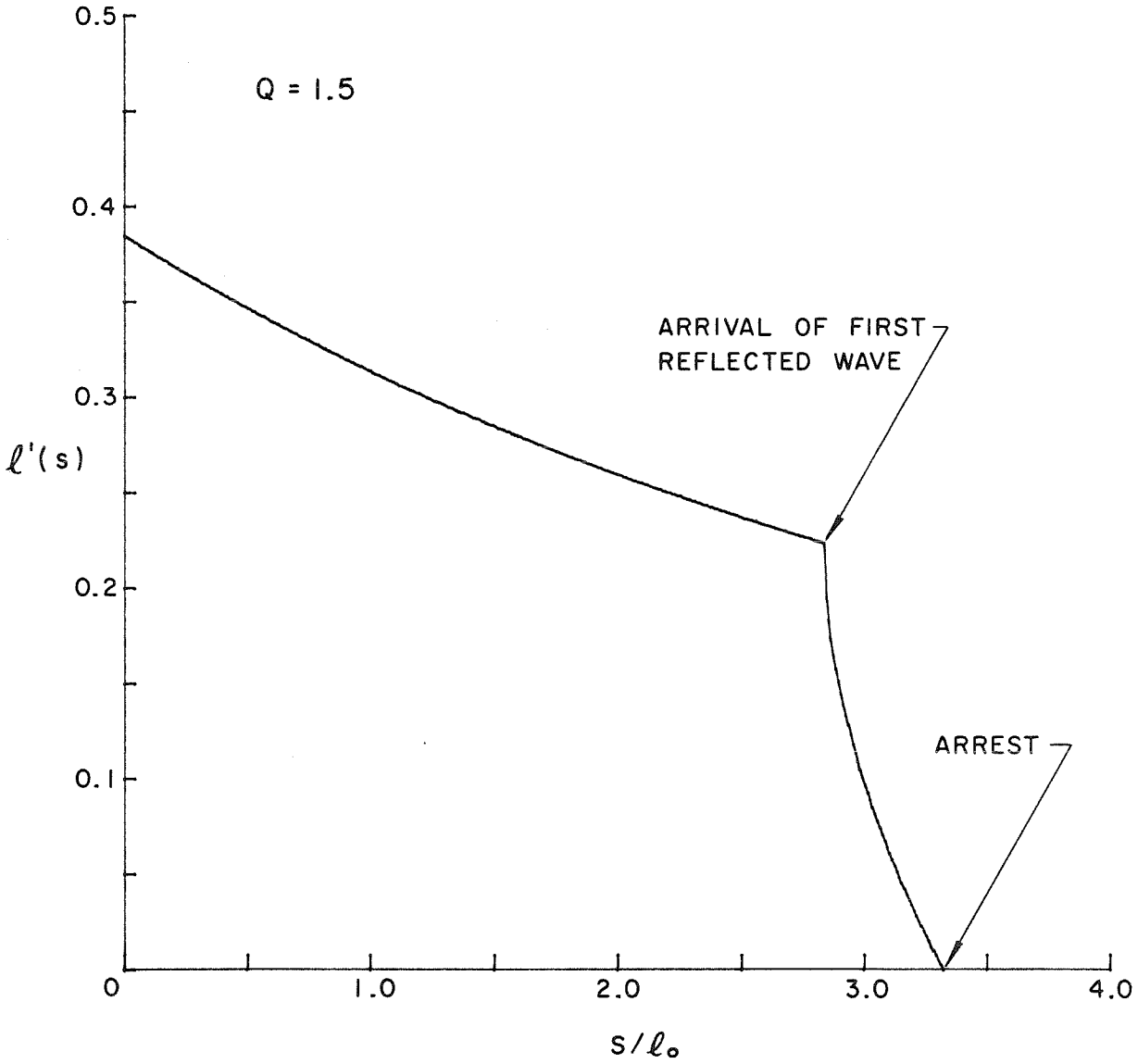

Figure 3. Normalized crack tip velocity $\ell'(s) = \dot{\ell}(t)/c$ as a function of $s/\ell_o = ct/\ell_o$, from the analytical solution.

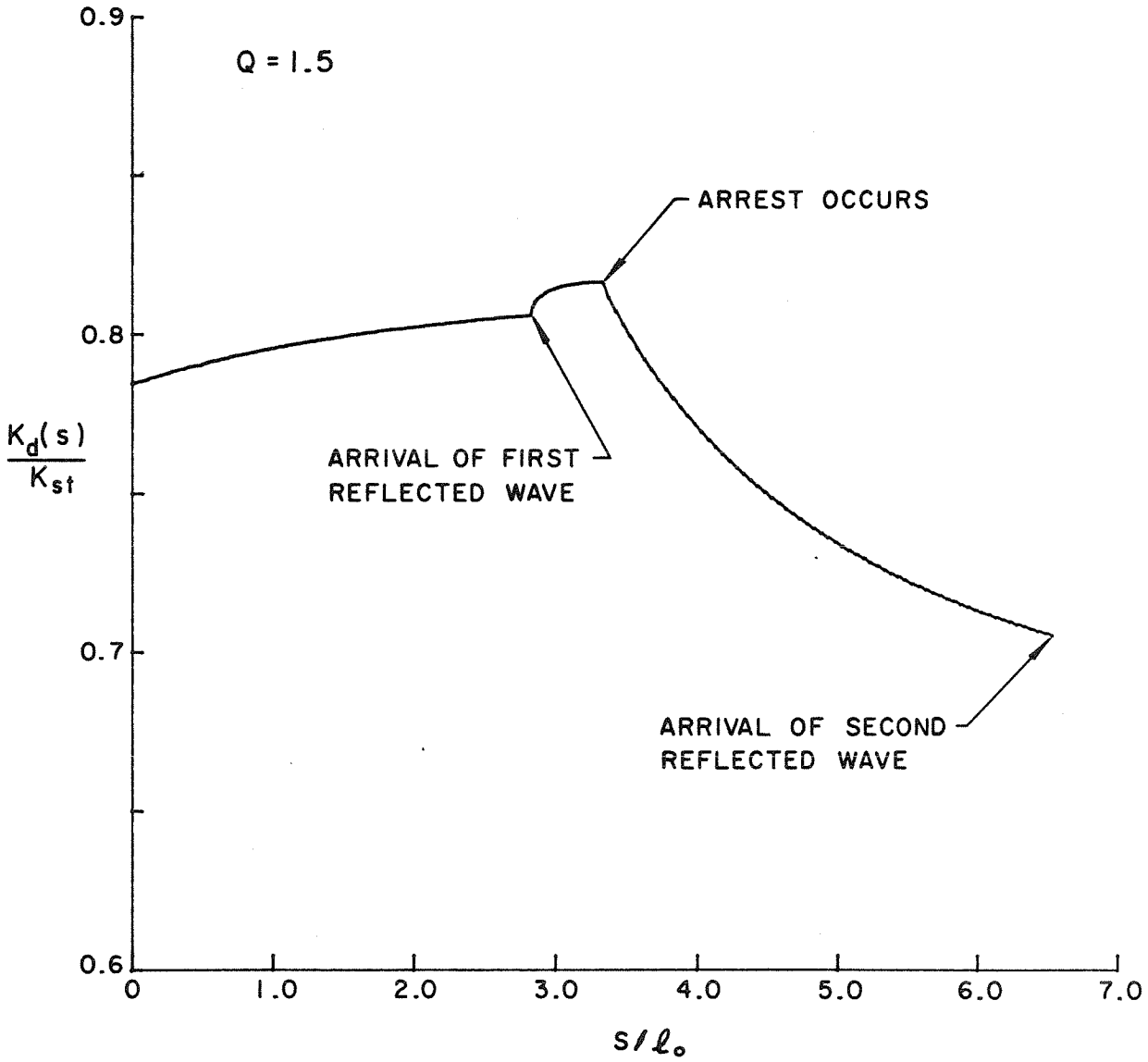

Figure 4. Normalized stress intensity factor $K_d(s)/K_{st}$ as a function of s/ℓ_o, from the analytical solution.

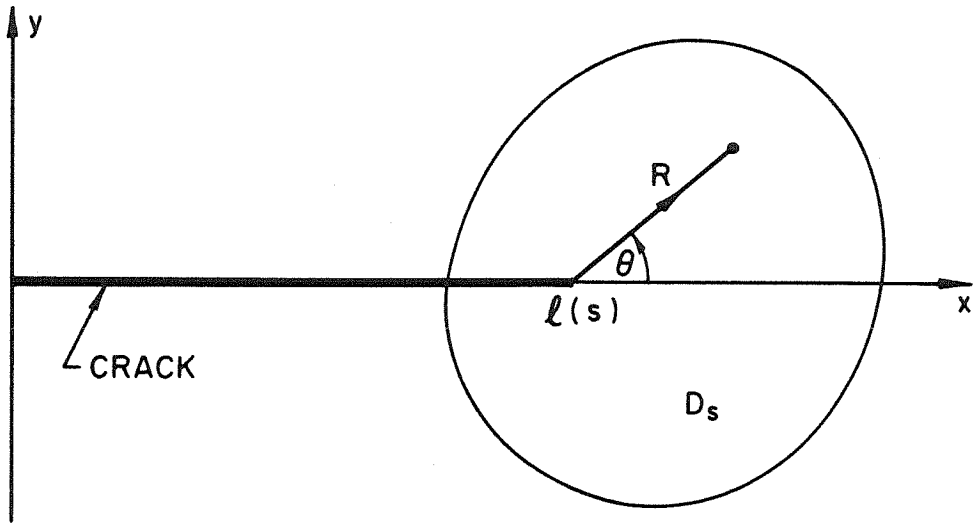

Figure 5. The local polar coordinates (R,θ) at the moving tip and the region D_s.

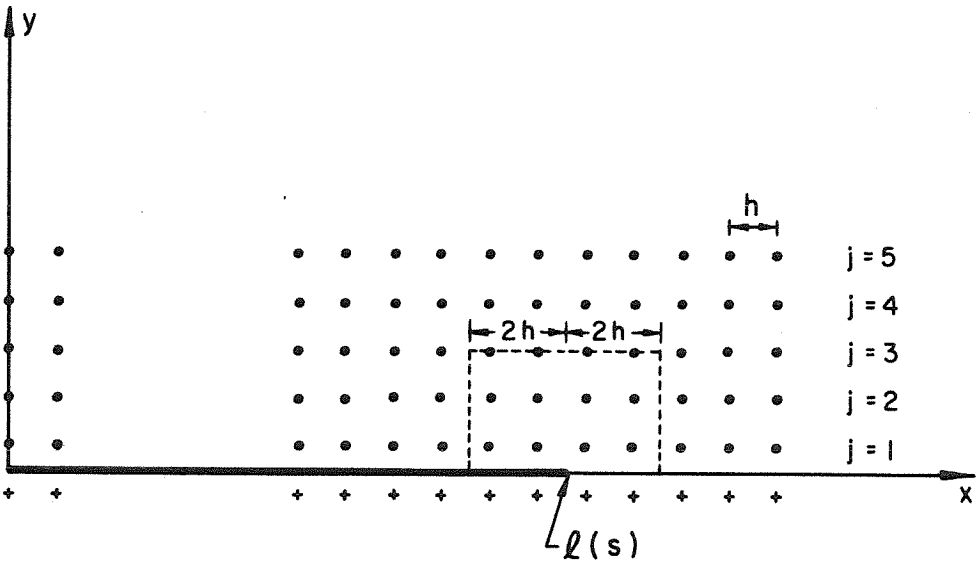

Figure 6. Arrangement of the grid points with respect to the crack: • — interior points, + — auxillary points. Dashed lines denote the upper-half of the contour C_s .

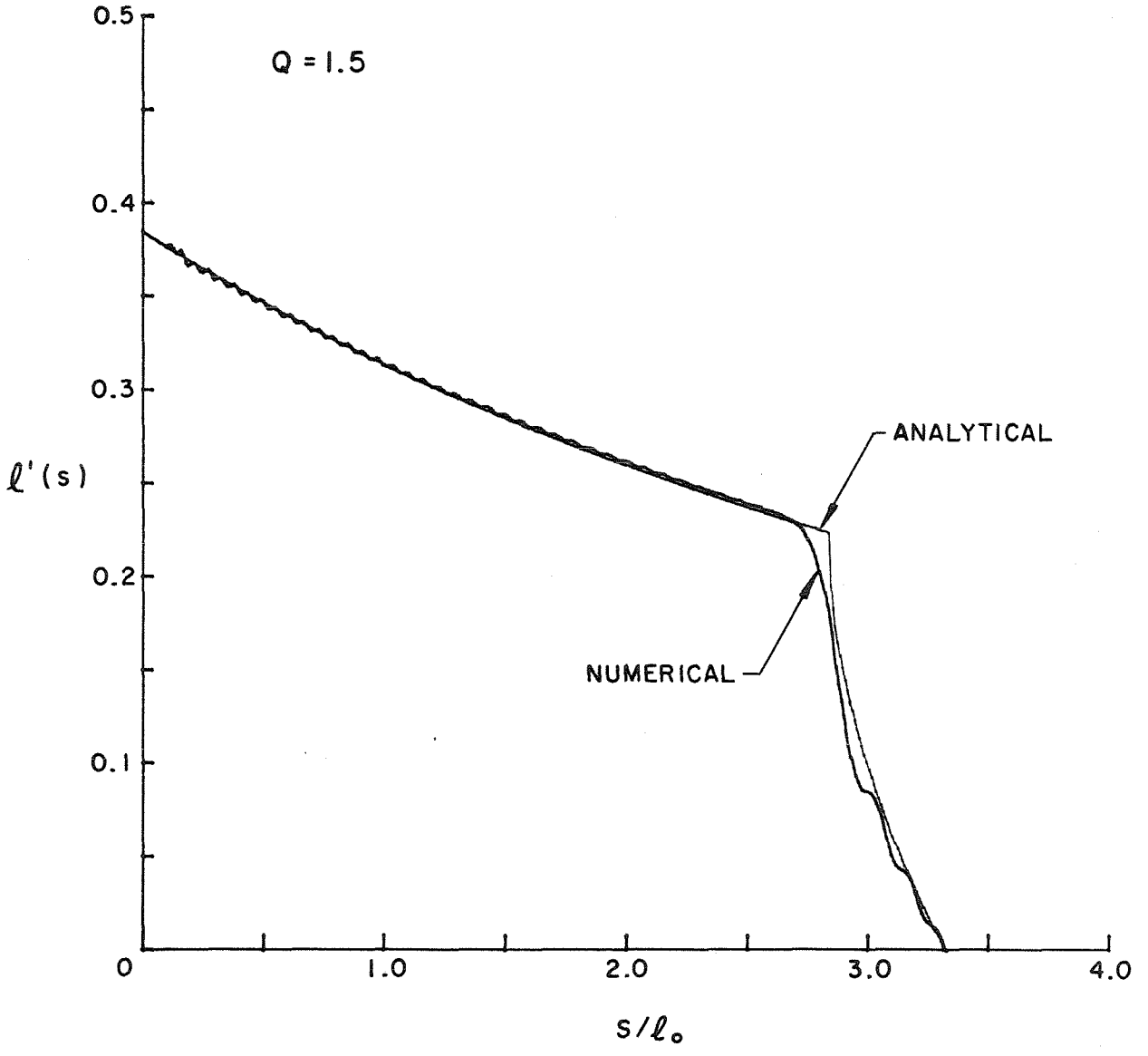

Figure 7. The normalized crack tip velocity $\ell'(s)$ calculated using finite differences and plotted as a function of s/ℓ_0. Analytical result also shown.

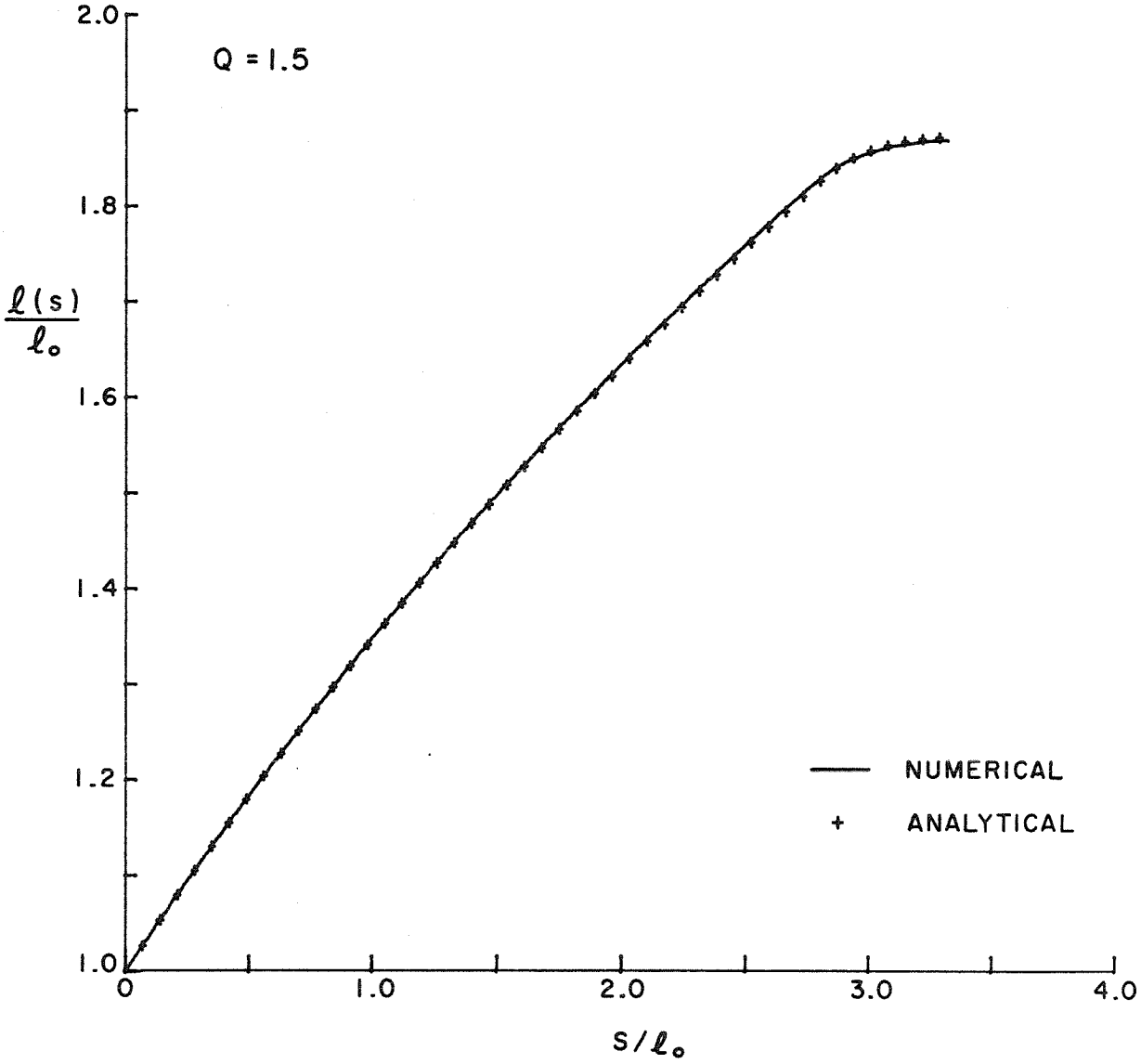

Figure 8. Normalized crack length $\ell(s)/\ell_0$ as a function of s/ℓ_0 .

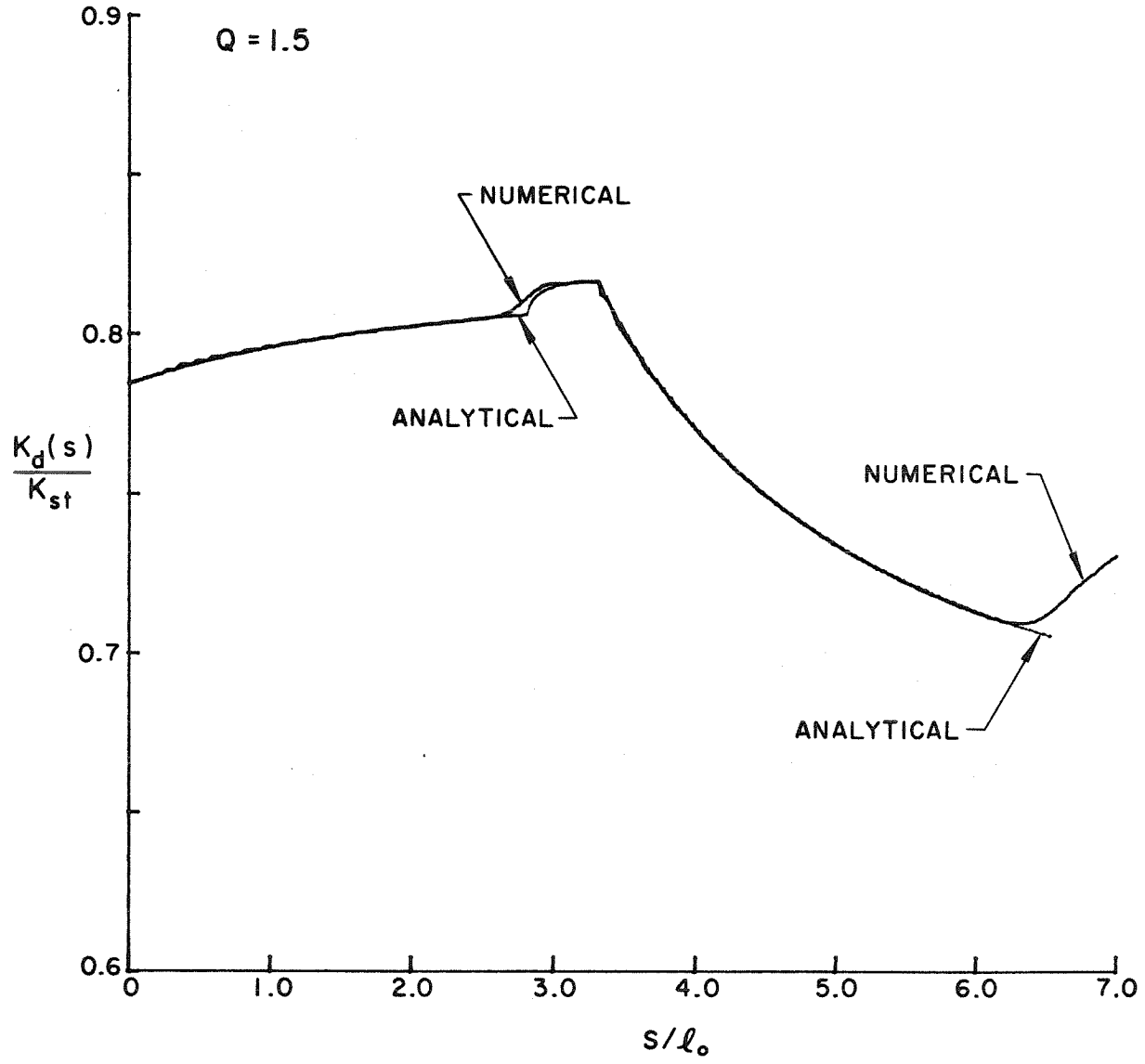

Figure 9. The normalized stress intensity factor $K_d(s)/K_{st}$ calculated using finite differences and plotted as a function of s/ℓ_o. Analytical result also shown.